THE JOURNAL OF PHYSICAL CHEMISTRY A

Article

Cite This: J. Phys. Chem. A 2019, 123, 4990−5004

pubs.acs.org/JPCA

First-Principles Calculation of Jahn−Teller Rotational Distortion Parameters

Published as part of The Journal of Physical Chemistry virtual special issue "Pacific Conference on Spectroscopy and Dynamics".

Ketan Sharma,[*,†] Scott Garner,[†,¶] Terry A. Miller,[*,†] and John F. Stanton[‡]

[†]Department of Chemistry and Biochemistry, The Ohio State University, Columbus, Ohio 43210, United States

[‡]Department of Chemistry, University of Florida, Gainesville, Florida 32611, United States

Supporting Information

ABSTRACT: A theoretical and computational framework is presented for the parameters h_1 and h_2 that appear in the rotational Hamiltonian for molecules subject to the Jahn−Teller effect. Expressions that relate h_1 and h_2 to first and second moments of the degenerate normal coordinates as well as derivatives of the inertia tensor are presented in detail for both cylindrical and Cartesian coordinate systems. The method is demonstrated for three situations in which experimental information about h_1 (and/or h_2) is available: the ground $^2E_1''$ and ^2E states of the cyclopentadienyl (C_5H_5) and methoxy (CH_3O) radicals, respectively, and the excited $^2E''$ state of the nitrate (NO_3) radical. Results for h_1 and h_2 parametrized by *ab initio* calculations exhibit good agreement with measured values, and they are demonstrably superior to those obtained with an approach based on first-order perturbation theory. The computational technology developed for h_1 and h_2 can be used to benchmark quantum chemistry calculations for molecules with Jahn−Teller effects and facilitate the analysis of their spectra.

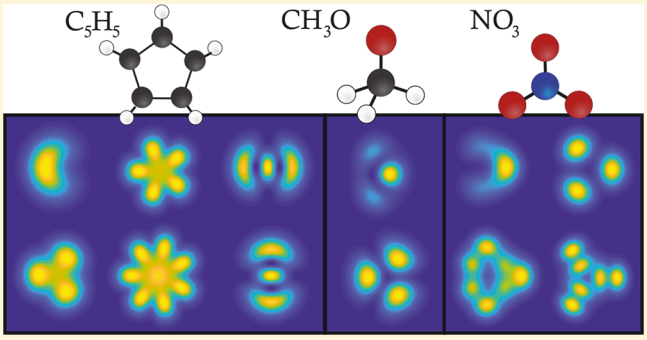

1. INTRODUCTION

Conical intersections (CIs) on potential energy surfaces[1−3] play an important role in molecules, affecting many aspects of their behavior that range from reaction dynamics to spectroscopic signatures.[4,5] While it was once thought that CIs dictated by symmetry (those which epitomize the Jahn−Teller (JT) effect) were far more common than those resulting from accidental degeneracies, it is now widely appreciated that intersections of two or more electronic states are ubiquitous. The last few decades have witnessed many advances made in the study of CIs, and this is now known to be a field of great relevance.

Studies of CIs are made from both the experimental and theoretical viewpoints. In the former area, the short passage time through the CI region in dynamical processes limits what can be learned from experiment, a consequence of the time-energy uncertainty principle. Theoretical calculations are also difficult, as the electronic problem must be solved in a multidimensional space, a fact that compromises the ability of standard single-reference quantum chemical methods (MP2, CCSD(T), etc.) to perform as they do for simpler problems.

The venerable Jahn−Teller problem,[6] where the CI is present because of symmetry, and for which the relatively low-energy dynamics tend to take place in the vicinity of the CI, is a convenient and appropriate case for the development and testing of theoretical and experimental methods for characterizing CIs. There is a long history of these studies, and many advances have been made in both theory and experiment.[7−11]

Experimental studies of the JT effect that provide information about the CIs are generally based on electronic spectroscopy. The levels measured experimentally can be fit by effective Hamiltonians (typically those characterized by linear and quadratic JT models). These Hamiltonians contain information about the adiabatic potential energy surfaces (PES) that comprise the CI, and also allow the prediction of other level positions that are not observed experimentally, due either to selection rules or to intrinsically weak transitions. Quantum chemical calculations can also be used to determine properties of CIs. Once an appropriate treatment of the electronic Hamiltonian is found (such as methods based on equation-of-motion coupled-cluster (EOM-CC)[12−14] or those based on complete active space self-consistent-field (CASSCF) calculations[15]), the adiabatic surfaces can be computed directly, and properties of the CI such as the JT stabilization energy (JTSE) (the energy difference between the minimum along the CI seam and the global minima of the JT-distorted

Received: April 10, 2019
Revised: May 15, 2019
Published: May 22, 2019

DOI: 10.1021/acs.jpca.9b03360
J. Phys. Chem. A 2019, 123, 4990−5004

molecule) and pseudorotation barriers are easily obtained. With more effort, quantum chemical calculations can be used to parametrize the aforementioned effective Hamiltonians, which can subsequently be diagonalized to obtain eigenvalues and eigenfunctions, the energy differences between the former giving frequencies in spectra and the latter characterizing the nature of the states involved.

Both experimental and theoretical studies of the JT effect are difficult, and it is desirable to find a way in which these distinctly different approaches can reinforce each other. It is interesting that even a very logical first step in this process—the calibration of theoretical calculations by comparison to experimental results—has turned out to be somewhat problematic. Specifically, it transpires that potential energy surface measures such as the JTSE and pseudorotation barriers that have been inferred from experimental level positions via the effective Hamiltonian approach sometimes agree quite poorly with those obtained directly by sophisticated quantum chemical calculations. While this is the expected result if the model Hamiltonian approach is unable to fit the experimental levels well, a recent work[16] by some of us shows that model Hamiltonian fits can provide quite poor representations of the computed adiabatic potential energy surfaces even when they provide excellent fits to level positions obtained from vibronic structure in spectra.

In this work, we explore how rotational structure in spectra can be used to compare experimental studies of JT molecules with theoretical calculations. The JT effect lowers the symmetry of a molecule by distorting its PES, which leads to the well-known departure of its vibrational (vibronic) structure from that of a typical harmonic oscillator model with small anharmonicities. The molecule's geometry at the PES minimum can be significantly distorted from its high symmetry configuration, which leads to rotational structure markedly different from that expected from the symmetric-top model appropriate to the highly symmetric geometry of the CI.

JT effects on the rotational structure of molecules were first considered by Child and co-workers.[17,18] Subsequently, Hougen[19] introduced two parameters, denoted h_1 and h_2, that characterize the effect of JT distortion on the rotational structure. While seminal, his analysis was strictly based on group theory, and therefore, it provided no physical explanation of the parameters and hence no basis for interpreting their experimental values or their calculation by quantum chemistry.

Shortly after Hougen's work, Watson[20] provided a physical explanation of two parameters comparable to h_1 and h_2 and correspondingly provided an approximate method for their calculation. His approach was very important in that it derived an effective rotational Hamiltonian that reflected the JT distortion of the PES. Not unexpectedly, given the era of Watson's work, his approach for computing the parameters has significant limitations. Specifically, his results are limited to a linear JT effect, which, moreover, has to be small since his approach was effectively a first order perturbation calculation, which would result in, at best, uncertain vibronic eigenfunctions if the JT distortions are significant. In addition, the power series expansion of the distortion parameters was truncated at first order. Finally, his work provided an approximate formula appropriate only for the zero-point level of the molecule.

Obviously tremendous computational advances have occurred in the meantime. As indicated earlier, vibronic eigenfunctions can now be determined using information from quantum chemistry calculations of the PES. It is the purpose of this paper to develop a procedure for predicting values of the h_1 and h_2 parameters from calculated vibronic Hamiltonians and to test the method against experimental results for several JT active molecules.

To accomplish this, we review the effective rotational Hamiltonian for JT active molecules and derive an approach to compute h_1 and h_2 from the results of quantum chemistry calculations. There have been spectral analyses[4,21] yielding values of h_1 and/or h_2 for several JT-active molecules, among these being cyclopentadienyl (C_5H_5), methoxy (CH_3O), and nitrate (NO_3) radicals. Here, we calculate parameters for these molecules and compare them to the experimental measurements. We also use our computational results to elucidate some general characteristics of h_1 and h_2 and relate these to the nature of the vibronic eigenfunctions.

The computational technology developed and described herein to compute h_1 and h_2 has significant potential for helping to calibrate the quality of theoretical calculations of the JT effect. Provided accurate experimental determination of the parameters is achieved (which however is not a trivial undertaking), then the quality of the calculated values can be unambiguously assessed, since they correspond precisely to what is measured. Thus, a comparison of calculated and experimental values of h_1 and h_2 is meaningful; in a sense, apples are being compared to apples and oranges to oranges. Historically, this is not the way that quantum chemical calculations of the JT effect have been benchmarked. It has rather been the *de facto* standard to compute potential energy surfaces and then compare these to properties of these surfaces (specifically the JTSE and pseudorotation barriers) extracted from experimentally based vibronic Hamiltonians. This is clearly a less straightforward comparison, as the surfaces are what is calculated but not really what is "measured" in the experiments and what goes on between the measurement of the energy levels and the construction (and necessary truncation) of the vibronic Hamiltonian can strongly undermine the fidelity of the resulting surface, as has recently been demonstrated.

2. THEORETICAL BACKGROUND AND DEVELOPMENT

2.1. Microscopic Rotational Hamiltonian. Since we are dealing with modification of rotational structure by the JT effect, a good starting place for our analysis is the general expression for the rotational kinetic energy of a nonrigid molecule, H_R, which is given as[19]

$$\boldsymbol{H}_R = [\boldsymbol{R}_\alpha \quad \boldsymbol{R}_\beta \quad \boldsymbol{R}_\sigma] \begin{bmatrix} \boldsymbol{B}_{\alpha\alpha} & \boldsymbol{B}_{\alpha\beta} & \boldsymbol{B}_{\alpha\sigma} \\ \boldsymbol{B}_{\beta\alpha} & \boldsymbol{B}_{\beta\beta} & \boldsymbol{B}_{\beta\sigma} \\ \boldsymbol{B}_{\sigma\alpha} & \boldsymbol{B}_{\sigma\beta} & \boldsymbol{B}_{\sigma\sigma} \end{bmatrix} \begin{bmatrix} \boldsymbol{R}_\alpha \\ \boldsymbol{R}_\beta \\ \boldsymbol{R}_\sigma \end{bmatrix} \tag{1}$$

The components of the rotational constant tensor, $\boldsymbol{B}$, are a function of nuclear coordinates ($\mathcal{R}_N$). The nuclear coordinates can be described in terms of a reference geometry ($\mathcal{R}_0$) and normal mode coordinates (q_N) with $q_N = 0$ at $\mathcal{R}_0$. $\boldsymbol{R}$ is the rotational angular momentum, defined as

$$\boldsymbol{R} \equiv \boldsymbol{J} - \boldsymbol{L} - \boldsymbol{G} - \boldsymbol{S} = \boldsymbol{N} - \boldsymbol{L} - \boldsymbol{G} \tag{2}$$

where $\boldsymbol{N} \equiv \boldsymbol{J} - \boldsymbol{S}$, with $\boldsymbol{J}$ and $\boldsymbol{S}$ being the total angular momentum of the molecule (excluding nuclear spin) and the electron spin, respectively. The electronic ($\boldsymbol{L}$) and the

DOI: 10.1021/acs.jpca.9b03360
J. Phys. Chem. A 2019, 123, 4990−5004

vibrational ($\boldsymbol{G}$) angular momenta are conventionally combined to form the "vibronic" angular momentum

$$\boldsymbol{\pi} \equiv \boldsymbol{L} + \boldsymbol{G} \tag{3}$$

The components α, β, and σ in eq 1, can be expressed in Cartesian coordinates (x, y and z) or cylindrical coordinates ($\pm = re^{\pm i\theta} = x \pm iy$ and $z = z$) which are related by a transformation matrix $\boldsymbol{U}$,

$$\boldsymbol{U} = \begin{bmatrix} 1 & i & 0 \\ 1 & -i & 0 \\ 0 & 0 & 1 \end{bmatrix} \quad \boldsymbol{U}^{-1} = \begin{bmatrix} \frac{1}{2} & \frac{1}{2} & 0 \\ -\frac{i}{2} & \frac{i}{2} & 0 \\ 0 & 0 & 1 \end{bmatrix} \tag{4}$$

The components of the inertia tensor are quadratic functions of the coordinates and therefore transform contravariantly (same as the coordinate system). The rotational tensor transforms as the inverse of the inertial tensor and hence covariantly. Therefore, the rotational tensor is transformed from Cartesian to cylindrical coordinates via

$$\boldsymbol{B}(+, -, z) = \frac{h}{8\pi^2 c}\boldsymbol{I}(+, -, z)^{-1} \tag{5a}$$

$$= \frac{h}{8\pi^2 c}(\boldsymbol{U}\boldsymbol{I}(x, y, z)\boldsymbol{U}^T)^{-1} \tag{5b}$$

$$= \frac{h}{8\pi^2 c}(\boldsymbol{U}^{-1})^T\boldsymbol{I}(x, y, z)^{-1}\boldsymbol{U}^{-1} \tag{5c}$$

$$= (\boldsymbol{U}^{-1})^T\boldsymbol{B}(x, y, z)\boldsymbol{U}^{-1} \tag{5d}$$

Explicitly

$$\begin{bmatrix} \boldsymbol{B}_{++} & \boldsymbol{B}_{+-} & \boldsymbol{B}_{+z} \\ \boldsymbol{B}_{-+} & \boldsymbol{B}_{--} & \boldsymbol{B}_{-z} \\ \boldsymbol{B}_{z+} & \boldsymbol{B}_{z-} & \boldsymbol{B}_{zz} \end{bmatrix} = \begin{bmatrix} \frac{1}{4}(\boldsymbol{B}_{xx} - \boldsymbol{B}_{yy} - i(\boldsymbol{B}_{yx} + \boldsymbol{B}_{xy})) & \frac{1}{4}(\boldsymbol{B}_{xx} + \boldsymbol{B}_{yy} + i(\boldsymbol{B}_{xy} - \boldsymbol{B}_{yx})) & \frac{1}{2}(\boldsymbol{B}_{xz} - i\boldsymbol{B}_{yz}) \\ \frac{1}{4}(\boldsymbol{B}_{xx} + \boldsymbol{B}_{yy} + i(\boldsymbol{B}_{yx} - \boldsymbol{B}_{xy})) & \frac{1}{4}(\boldsymbol{B}_{xx} - \boldsymbol{B}_{yy} + i(\boldsymbol{B}_{yx} + \boldsymbol{B}_{xy})) & \frac{1}{2}(\boldsymbol{B}_{xz} + i\boldsymbol{B}_{yz}) \\ \frac{1}{2}(\boldsymbol{B}_{zx} - i\boldsymbol{B}_{zy}) & \frac{1}{2}(\boldsymbol{B}_{zx} + i\boldsymbol{B}_{zy}) & \boldsymbol{B}_{zz} \end{bmatrix} \tag{6}$$

The inverse relationship is

$$\boldsymbol{B}(x, y, z) = \boldsymbol{U}^T\boldsymbol{B}(+, -, z)\boldsymbol{U} \tag{7}$$

The rotational Hamiltonian in eq 1 can be recast in terms of raising and lowering operators

$$\boldsymbol{N}_\pm = \boldsymbol{N}_x \pm i\boldsymbol{N}_y \tag{8}$$

$$\boldsymbol{\pi}_\pm = \boldsymbol{\pi}_x \pm i\boldsymbol{\pi}_y \tag{9}$$

Using eqs 1−3 and these operators, we can rewrite H_R as

$$\boldsymbol{H}_R = (\boldsymbol{N} - \boldsymbol{\pi})^T\boldsymbol{B}(\boldsymbol{N} - \boldsymbol{\pi}) = \boldsymbol{N}^T\boldsymbol{B}\boldsymbol{N} - (\boldsymbol{N}^T\boldsymbol{B}\boldsymbol{\pi} + \boldsymbol{\pi}^T\boldsymbol{B}\boldsymbol{N}) + \boldsymbol{\pi}^T\boldsymbol{B}\boldsymbol{\pi} = \boldsymbol{H}_R^0 + \boldsymbol{H}_R^1 + \boldsymbol{H}_R^2 \tag{10}$$

where

$$\boldsymbol{H}_R^0 = \boldsymbol{B}_{-+}\boldsymbol{\pi}_-\boldsymbol{\pi}_+ + \boldsymbol{B}_{+-}\boldsymbol{\pi}_-\boldsymbol{\pi}_+ + \boldsymbol{B}_{--}\boldsymbol{\pi}_+^2 + \boldsymbol{B}_{+z}\boldsymbol{\pi}_-\boldsymbol{\pi}_z + \boldsymbol{B}_{z+}\boldsymbol{\pi}_-\boldsymbol{\pi}_z + \boldsymbol{B}_{-z}\boldsymbol{\pi}_+\boldsymbol{\pi}_z + \boldsymbol{B}_{z-}\boldsymbol{\pi}_+\boldsymbol{\pi}_z + \boldsymbol{B}_{zz}\boldsymbol{\pi}_z^2 + \boldsymbol{B}_{++}\boldsymbol{\pi}_-^2 \tag{11}$$

$$\boldsymbol{H}_R^1 = -2\boldsymbol{B}_{zz}\boldsymbol{N}_z\boldsymbol{\pi}_z - \boldsymbol{B}_{-+}\boldsymbol{N}_+\boldsymbol{\pi}_- - \boldsymbol{B}_{-+}\boldsymbol{N}_-\boldsymbol{\pi}_+ - \boldsymbol{B}_{+-}\boldsymbol{N}_+\boldsymbol{\pi}_- - \boldsymbol{B}_{+-}\boldsymbol{N}_-\boldsymbol{\pi}_+ - \boldsymbol{B}_{+z}\boldsymbol{N}_z\boldsymbol{\pi}_- - \boldsymbol{B}_{z+}\boldsymbol{N}_z\boldsymbol{\pi}_- - \boldsymbol{B}_{+z}\boldsymbol{N}_-\boldsymbol{\pi}_z - \boldsymbol{B}_{z+}\boldsymbol{N}_-\boldsymbol{\pi}_z - \boldsymbol{B}_{-z}\boldsymbol{N}_z\boldsymbol{\pi}_+ - \boldsymbol{B}_{z-}\boldsymbol{N}_z\boldsymbol{\pi}_+ - \boldsymbol{B}_{-z}\boldsymbol{N}_+\boldsymbol{\pi}_z - \boldsymbol{B}_{z-}\boldsymbol{N}_+\boldsymbol{\pi}_z - 2\boldsymbol{B}_{++}\boldsymbol{N}_-\boldsymbol{\pi}_- - 2\boldsymbol{B}_{--}\boldsymbol{N}_+\boldsymbol{\pi}_+ \tag{12}$$

$$\boldsymbol{H}_R^2 = \boldsymbol{B}_{-+}\boldsymbol{N}_-\boldsymbol{N}_+ + \boldsymbol{B}_{zz}\boldsymbol{N}_z^2 + \boldsymbol{B}_{+-}\boldsymbol{N}_-\boldsymbol{N}_+ + \boldsymbol{B}_{++}\boldsymbol{N}_-^2 + \boldsymbol{B}_{--}\boldsymbol{N}_+^2 + \boldsymbol{B}_{+z}\boldsymbol{N}_-\boldsymbol{N}_z + \boldsymbol{B}_{z+}\boldsymbol{N}_-\boldsymbol{N}_z + \boldsymbol{B}_{-z}\boldsymbol{N}_+\boldsymbol{N}_z + \boldsymbol{B}_{z-}\boldsymbol{N}_+\boldsymbol{N}_z \tag{13}$$

The first term, H_R^0, in the rovibronic Hamiltonian is clearly independent of $\boldsymbol{N}$, while the second, H_R^1, and third, H_R^2, contain operators that are linear and quadratic in $\boldsymbol{N}$, respectively. H_R^0 does not contribute directly to the rotational spectrum and is ignored. The terms linear in $\boldsymbol{N}$ constitute the Coriolis coupling terms. The part of the Hamiltonian upon which we will concentrate in this paper is the one quadratic in $\boldsymbol{N}$, which is the most significantly affected by JT interactions and gives rise to the distortion parameters h_1 and h_2.

2.2. Spin-Vibronic and Rotational Basis Sets. A judicious choice of basis set is extremely helpful both to minimize the computational effort and to provide the best physical picture of the mechanisms responsible for observed effects in spectra resulting from JT interactions. We will refer to the overall basis set as rotational spin vibronic $|\mathrm{RSV}\rangle$, i.e.

$$|\mathrm{RSV}\rangle = |\mathrm{SV}\rangle|\mathrm{R}\rangle \tag{14}$$

For the purposes of this paper, where the molecules are subject to nonzero JT interactions, the explicit rotational basis function is taken as a symmetric top with suitable extension for nonrigidity since both require a proper or improper rotational symmetry axis of order three or higher.[22] (While a spherical top is also possible, its rotational basis functions can be trivially derived from those of the symmetric top.)

The coupling of the electronic spin to the rotational angular momentum can be described by either of two conventional models referred to as Hund's case a and case b. The former has good quantum numbers $|JPS\Sigma\rangle$. The total angular momentum, $\boldsymbol{J}$, of the molecule has a projection, P, along the z axis. The projection, P_s, of $\boldsymbol{S}$ upon the same axis is Σ. The case b like basis functions can be written $|JSNK\rangle$ in which the total angular is $\boldsymbol{J} = \boldsymbol{N} + \boldsymbol{S}$ and K is the projection of $\boldsymbol{N}$ along the symmetric top (z) axis. As will be explained in more detail below, generally the better choice for large spin−orbit coupling is case a while case b is preferable for small coupling. Of course the case a or b sets span the same space, and they are related to one another by a unitary transformation:[23]

DOI: 10.1021/acs.jpca.9b03360
J. Phys. Chem. A 2019, 123, 4990−5004

$$|JSNK\rangle = \sum_{\Sigma,P} (-1)^{-J+P+2S}\sqrt{2N+1}\begin{pmatrix} J & N & S \\ P & -K & -\Sigma \end{pmatrix} |JPS\Sigma\rangle \tag{15}$$

For a doublet state, and Hund's case b basis functions, this relationship condenses to,

$$\left|J = N \pm \frac{1}{2}, SKN\right\rangle = \sqrt{\frac{J+K+1/2}{2J+1}}\left|JP = K \pm \frac{1}{2}\right\rangle \left|S\Sigma = \pm\frac{1}{2}\right\rangle \pm \sqrt{\frac{J+K+1/2}{2J+1}}\left|JP = K \mp \frac{1}{2}\right\rangle \left|S\Sigma = \mp\frac{1}{2}\right\rangle \tag{16}$$

It is important to pair $|SV\rangle$ and $|R\rangle$ basis functions appropriately and to do that we need to characterize the spin-vibronic basis functions by considering the Hamiltonian

$$H_T = H_e^0 + H_{JT} + H_{SO} \tag{17}$$

In the absence of JT-type vibronic interactions, i.e., $H_{JT} = 0$, H_e^0 can be taken to have diabatic eigenfunctions, at fixed $\mathcal{R}_0$, which we write as $|\Lambda_i\rangle$ where Λ_i is a signed integer that denotes their rotational transformation property, $e^{i\Lambda\theta}$, $(\theta = \frac{2\pi}{n})$, about the highest symmetry axis, z, of order n.

The Hamiltonian, H_{JT}, has been studied in great detail.[24,25] For a doubly degenerate state, H_{JT} can be represented as a 2×2 matrix in the electronic basis, with the harmonic, vibrational basis projected on each Λ state[26]

$$H_{JT} = \begin{bmatrix} T_N & 0 \\ 0 & T_N \end{bmatrix} + \begin{bmatrix} V_{\tilde{A}_+} & V_{\tilde{A}_{+-}} \\ V_{\tilde{A}_{-+}} & V_{\tilde{A}_-} \end{bmatrix} \tag{18}$$

Here T_N is the nuclear kinetic energy, excluding rotation, and (through quadratic terms)

$$V_{\tilde{A}_+} = V_{\tilde{A}_-} = V_0 + \frac{1}{2}\sum_{i=1}^{f}\omega_i q_i^2 + \frac{1}{2}\sum_{i=f+1}^{f+g}\omega_i q_{i+}q_{i-} + \sum_{i=1}^{f} d_i q_i \tag{19a}$$

The form of $V_{\tilde{A}_{+-}}$ depends on the symmetry of the electronic state. We give results later for ^2E electronic states of C_{3v} and D_{3h} symmetry for which

$$V_{\tilde{A}_{+-}} = \sum_{i=f+1}^{f+g} k_i q_{i-} + \sum_{i=f+1}^{f+g} g_{ii} q_{i+}^2 + \sum_{i=f+1}^{f+g-1}\sum_{j=i+1}^{f+g} g_{ij} q_{i+}q_{j+} + \sum_{i=1}^{f}\sum_{j=f+1}^{f+g} b_{ij} q_i q_{j-} \tag{19b}$$

and for the $^2E_1''$ state of D_{3h}, for which

$$V_{\tilde{A}_{+-}} = \sum_{i=f+1}^{f+g} k_i q_{i+} + \sum_{i=f+1}^{f+g} g_{ii} q_{i-}^2 + \sum_{i=f+1}^{f+g-1}\sum_{j=i+1}^{f+g} g_{ij} q_{i-}q_{j-} + \sum_{i=1}^{f}\sum_{j=f+1}^{f+g} b_{ij} q_i q_{j+} \tag{19c}$$

In the above, f is the total number of nondegenerate modes and g is the total number of degenerate modes ($f + 2g = 3N - 6$). V_0 is the (degenerate) eigenenergy of H_e which can be dropped. We express the other parameters in terms of derivatives of the adiabatic electronic potential energy surface (PES) with respect to the normal coordinates in cylindrical form. The expansion has been carried out to the second power, and the explicit parameter definitions are found in Table 1. It is of note that d_i is nonzero only for totally symmetric modes and only if the expansion is carried out at a nonstationary point of the diabatic potential.

Table 1. Harmonic Frequency and Jahn Teller Coupling Parameters in Cylindrical Coordinates[a]

Symbols	Description	Definition
d_i	gradient along symmetric mode	$\frac{\partial}{\partial q_i}(\langle\Lambda_\pm\|\mathcal{H}_e\|\Lambda_\pm\rangle)\Big\|_{R_0}$
k_i	linear JT coupling constant	$\frac{\partial}{\partial q_{i,\pm}}(\langle\Lambda_\pm\|\mathcal{H}_e\|\Lambda_\mp\rangle)\Big\|_{R_0}$
λ_i	harmonic force constant for JT active mode	$\frac{\partial^2}{\partial q_{i,+}\partial q_{i,-}}(\langle\Lambda_\pm\|\mathcal{H}_e\|\Lambda_\pm\rangle)\Big\|_{R_0}$
λ_i'	harmonic force constant for JT inactive mode	$\frac{\partial^2}{\partial q_i^2}(\langle\Lambda_\pm\|\mathcal{H}_e\|\Lambda_\pm\rangle)\Big\|_{R_0}$
g_{ii}	quadratic JT coupling constant	$\frac{\partial^2}{\partial q_{i,\pm}^2}(\langle\Lambda_\pm\|\mathcal{H}_e\|\Lambda_\mp\rangle)\Big\|_{R_0}$
g_{ij}	cross-quadratic JT coupling constant	$\frac{\partial^2}{\partial q_{i,\pm}\partial q_{j,\pm}}(\langle\Lambda_\pm\|\mathcal{H}_e\|\Lambda_\mp\rangle)\Big\|_{R_0}$
b_{ij}	bilinear JT coupling constant	$\frac{\partial^2}{\partial q_{i,\pm}\partial q_j}(\langle\Lambda_\pm\|\mathcal{H}_e\|\Lambda_\mp\rangle)\Big\|_{R_0}$

[a] $\langle\Lambda|\mathcal{H}_e|\Lambda'\rangle$ is the electronic potential at the symmetric configuration denoted by R_0, which includes Coulomb interaction, exchange interaction etc.

The effective Hamiltonian H_{SO} for spin−orbit interaction can be written with sufficient generality as[24]

$$\boldsymbol{H}_{SO} = a_z L_z S_z + \frac{1}{2}a_\perp(L_+S_- + L_-S_+) \tag{20}$$

It is worthwhile to note that a_z and $a_\perp$, like the rotational parameters, $B_{\alpha\alpha}$, are operators in the vibronic space. H_{SO} may be combined with H_{JT} or incorporated into the rotational Hamiltonian, typically depending upon its relative magnitude compared to H_{JT} and H_R.

In the absence of H_{SO}, H_{JT} can be represented in a direct-product, vibronic basis, $|D_p\rangle_i$, where

$$|D_p\rangle_i = |\Lambda_i\rangle \otimes \prod_{m=1}^{f}|v_{m,i}\rangle \otimes \prod_{m=f+1}^{f+g}|v_{m,i}, l_{m,i}\rangle \tag{21}$$

The matrix elements of the operators in eq 19 in this basis are presented in the Supporting Information. The Hamiltonian matrix is truncated by limiting the vibrational part of the basis to a reasonable value (v_{max}), and the Lanczos algorithm is used

DOI: 10.1021/acs.jpca.9b03360
J. Phys. Chem. A 2019, 123, 4990−5004

to calculate its eigenvalues and eigenvectors. The details for truncation of the matrix and convergence of eigenvalues are different for each molecule and are discussed subsequently. The eigenvectors of the Hamiltonian are a linear combination of basis functions and are further characterized on the basis of symmetry. The vibronic eigenfunction, $|V\rangle$, can be uniquely labeled by its spatial symmetry, $E^{\kappa}_{s\pm}$ (see the Supporting Information), and energy position, denoted by n starting at zero for the lowest energy state and increasing monotonically, i.e.

$$|V\rangle = |n, E^{\kappa}_{s\pm}\rangle = \sum_i C^n_i |\Lambda_i\rangle \prod_{m=1}^{f} |v_{m,i}\rangle \prod_{m=f+1}^{f+g} |v_{m,i}, l_{m,i}\rangle \tag{22}$$

For small H_{SO}, it can be included in the rotational Hamiltonian and the $|V\rangle$ basis is paired with a case b like rotational basis $|JSNK\rangle$ which incorporates the spin S and its space-fixed projection $P_s = M_s$.

If H_{SO} is comparable or larger than H_{JT}, the appropriate combination is a case a $|JPS\Sigma\rangle$ rotational basis with a complete spin-vibronic basis, i.e. $|SV\rangle = |n, \tilde{E}^{\kappa}_{s\pm}, \Sigma\rangle$, where now $P_s = \Sigma$, the spin's projection on the molecule's symmetry axis. The eigenfunction $|n, \tilde{E}^{\kappa}_{s\pm}, \Sigma\rangle$ of $(H_{JT} + H_{SO})$ transforms as an irreducible representation of the symmetry group $\tilde{E}^{\kappa}_{s\pm}$ of the molecule including electron spin, $\pm$ depicting the two Kramers components of a degenerate vibronic level. The spin-vibronic eigenstates are

$$|SV\rangle \equiv \Psi^{SV} \equiv |n, \tilde{E}^{\kappa}_{s\pm}, \Sigma\rangle = \sum_{i,k} C^n_{i,k} |\Lambda_i\rangle |S\Sigma\rangle \prod_{m=p+1}^{f+g} |v_{m,k}, l_{m,k}\rangle \prod_{m=1}^{f} |v_{m,k}\rangle \tag{23}$$

In either case, the coefficients, C^n, of the eigenkets can be obtained from our spin−orbit coupling Jahn−Teller (SOCJT2) software[27,28] assuming suitable values are input for the JT and SO parameters (zero for the latter in case b). These eigenvectors are used to calculate h_1 and h_2, as described in Section 2.3.

2.3. The JT Parameters, h_1 and h_2, in the Effective Rovibronic Hamiltonian. To obtain an effective rotational Hamiltonian for a given spin-vibronic level, we need to expand the rotational tensor components of H^2_R (eq 13) in terms of the normal coordinates. The inertial tensor, and therefore the rotational tensor (eq 5), is a function of the nuclear coordinates, $\mathcal{R}$. The matrix elements of the rotational tensor component $B_{\alpha\beta}$ in the vibronic basis (eq 21):

$$\langle \phi_{i'} \langle \boldsymbol{B_{\alpha\beta}} | \phi_i \rangle = \langle \Lambda_{i'} | \prod_{m=1}^{f} \langle v_{m,i'} | \prod_{m=f+1}^{f+g} \langle v_{m,i'}, l_{m,i'} | \boldsymbol{B_{\alpha\beta}} | \Lambda_i \rangle \prod_{m=1}^{f} |v_{m,i}\rangle \prod_{m=f+1}^{f+g} |v_{m,i}, l_{m,i}\rangle \tag{24}$$

are treated as follows. In the diabatic representations, the electronic basis functions ($|\Lambda_i\rangle$) are fixed (to those at $\mathcal{R}_0$) and only the vibrational part has $\mathcal{R}$ dependence.

$$\begin{aligned}\langle \phi_{i'} | \boldsymbol{B_{\alpha\beta}} | \phi_i \rangle &= \delta_{\Lambda_{i'},\Lambda_i} \prod_{m=1}^{f} \langle v_{m,i'} | \prod_{m=f+1}^{f+g} \langle v_{m,i'}, l_{m,i'} | \boldsymbol{B_{\alpha\beta}} | \prod_{m=1}^{f} |v_{m,i}\rangle \\ &\prod_{m=f+1}^{f+g} |v_{m,i}, l_{m,i}\rangle = \delta_{\Lambda_{i'},\Lambda_i} [B_{\alpha\beta}|_{R_0} \prod_{m=1}^{g} \delta_{v_{m,i'},v_{m,i}} \prod_{m=f+1}^{f+g} \delta_{l_{m,i'},l_{m,i}} \\ &+ \sum_{j=1}^{f} \sum_{r=+,-} \left.\frac{\partial B_{\alpha\beta}}{\partial q_{j,r}}\right|_{R_0} \prod_{m=1}^{f} \langle v_{m,i'} | \prod_{m=f+1}^{f+g} \langle v_{m,i'}, l_{m,i'} | \boldsymbol{q_{j,r}} \\ &\prod_{m=1}^{f} |v_{m,i}\rangle \prod_{m=f+1}^{f+g} |v_{m,i}, l_{m,i}\rangle \\ &+ \frac{1}{2} \sum_{j} \sum_{k>i} \sum_{r_j=+,-} \sum_{r_k=+,-} \left.\frac{\partial^2 B_{\alpha\beta}}{\partial q_{j,r_j} \partial q_{k,r_k}}\right|_{R_0} \prod_{m=1}^{f} \langle v_{m,i'} | \\ &\prod_{m=f+1}^{f+g} \langle v_{m,i'}, l_{m,i'} | \boldsymbol{q_{j,r_j} q_{k,r_k}} \prod_{m=1}^{f} |v_{m,i}\rangle \prod_{m=f+1}^{f+g} |v_{m,i}, l_{m,i}\rangle + \ldots]\end{aligned} \tag{25}$$

We have omitted the sum over contributions involving nondegenerate modes as their nonlinear contribution to h_i tends to be negligible, but an extension of this expansion to include nondegenerate modes is trivial.

Be definition, in the principal axis system (PAS) the values of the components of the rigid-rotor rotational tensor at $\mathcal{R}_0$ are nonzero only for the diagonal terms, $B_{\alpha\alpha}$, which define the rotational constants for the effective Hamiltonian. The expansion of the other elements of the rotational tensor, $B_{\alpha\beta}$, both diagonal and off-diagonal, start with the term linear in q.

In the Supporting Information, we derive the symmetry properties of the various terms of H^2_R and the rotational eigenfunctions. Only the operators B_{zz}, B_{+-}, and B_{-+} transform as the totally symmetric representation of the molecular symmetry group and have nonvanishing contributions in the "standard" symmetric top rotational Hamiltonian model. This is because these are the only operators that have nonvanishing matrix elements within the + or - components of a degenerate vibronic level, i.e., $|E^{\kappa}_{s\pm}\rangle$.

Group theoretically, the remaining terms of H^2_R may have nonzero off-diagonal matrix elements between the components of a vibronic level of the molecule considered. $B_{\pm\pm}$ transforms as $E_{2\pm}{}'$ for C_5H_5 and therefore has nonzero matrix elements of the form $\langle E_{1\pm}{}'|B_{\pm\pm}|E_{1\mp}{}'\rangle$. Similarly, for NO_3 and CH_3O, $B_{\pm\pm}$ transforms as $E^{\kappa}_{\pm}$ and $E_{\pm}$ respectively, which leads to nonzero matrix elements of the form $\langle E_{\mp}{}'|B_{\pm\pm}|E_{\pm}{}'\rangle$ and $\langle E_{\mp}|B_{\pm\pm}|E_{\pm}\rangle$ for the two molecules. $B_{z\pm}$ and $B_{\pm z}$ transform as $E''_{1\pm}$ for C_5H_5 and $E''_{\pm}$ for NO_3 and has no nonvanishing matrix elements. This leads to vanishing of h_2 for such molecules. On the other hand, for CH_3O, $B_{\pm z}$ and $B_{z\pm}$ transform as $E_{\pm}$ and have nonvanishing matrix elements of the form $\langle E_{\pm}|B_{z\pm}|E_{\mp}\rangle = \langle E_{\mp}|B_{\mp z}|E_{\pm}\rangle$. Application of these principles leads to explicit equations for the first (h'_i) and second (h''_i) contributions to h_1 and h_2, i.e., $h_i = h'_i + h''_i$, in terms of their expectation values over specific (spin-) vibronic eigenkets. We can express the matrix elements of h_1 in terms of degenerate vibronic eigenfunctions which are of the following form:

$$|E^{\kappa}_{s\pm}\rangle = \sum_i C_i |\pm\Lambda_i\rangle \prod_{m=1}^{p} |v_{m,i}, \pm l_{m,i}\rangle \tag{26}$$

DOI: 10.1021/acs.jpca.9b03360
J. Phys. Chem. A 2019, 123, 4990−5004

Therefore, we can write the first order contribution to h_1 (h_1') as

$$h_1' = \sum_i \sum_{r=+,-} \left.\frac{\partial B_{++}}{\partial q_{i,r}}\right|_{R_0} \langle E_{s+}^{\kappa}|\boldsymbol{q}_{i,r}|E_{s-}^{\kappa}\rangle = \sum_i \sum_{r=+,-} \left.\frac{\partial B_{--}}{\partial q_{i,r}}\right|_{R_0} \langle E_{s-}^{\kappa}|\boldsymbol{q}_{i,r}|E_{s+}^{\kappa}\rangle \tag{27}$$

The rotational constant derivatives are evaluated at the fixed nuclear configuration $\mathcal{R}_0$.

Correspondingly

$$h_1'' = \frac{1}{2}\sum_{\substack{i,j\\ i\le j}} \sum_{r_i=+,-} \sum_{r_j=+,-} \left.\frac{\partial^2 B_{++}}{\partial q_{i,r_i}\partial q_{j,r_j}}\right|_{R_0} \langle E_{s+}^{\kappa}|\boldsymbol{q}_{i,r_i}\boldsymbol{q}_{j,r_j}|E_{s-}^{\kappa}\rangle = \frac{1}{2}\sum_{\substack{i,j\\ i\le j}} \sum_{r_i=+,-} \sum_{r_j=+,-} \left.\frac{\partial^2 B_{--}}{\partial q_{i,r_i}\partial q_{j,r_j}}\right|_{R_0} \langle E_{s-}^{\kappa}|\boldsymbol{q}_{i,r_i}\boldsymbol{q}_{j,r_j}|E_{s+}^{\kappa}\rangle \tag{28}$$

Similarly for h_2'

$$h_2' = \sum_i \sum_{r=+,-} \left.\frac{\partial B_{-z}}{\partial q_{i,r}}\right|_{R_0} \langle E_{s+}^{\kappa}|\boldsymbol{q}_{i,r}|E_{s-}^{\kappa}\rangle = \sum_i \sum_{r=+,-} \left.\frac{\partial B_{+z}}{\partial q_{i,r}}\right|_{R_0} \langle E_{s-}^{\kappa}|\boldsymbol{q}_{i,r}|E_{s+}^{\kappa}\rangle \tag{29}$$

and for h_2''

$$h_2'' = \frac{1}{2}\sum_{\substack{i,j\\ i\le j}} \sum_{r_i=+,-} \sum_{r_j=+,-} \left.\frac{\partial^2 B_{-z}}{\partial q_{i,r_i}\partial q_{j,r_j}}\right|_{R_0} \langle E_{s+}^{\kappa}|\boldsymbol{q}_{i,r_i}\boldsymbol{q}_{j,r_j}|E_{s-}^{\kappa}\rangle = \frac{1}{2}\sum_{\substack{i,j\\ i\le j}} \sum_{r_i=+,-} \sum_{r_j=+,-} \left.\frac{\partial^2 B_{+z}}{\partial q_{i,r_i}\partial q_{j,r_j}}\right|_{R_0} \langle E_{s-}^{\kappa}|\boldsymbol{q}_{i,r_i}\boldsymbol{q}_{j,r_j}|E_{s+}^{\kappa}\rangle \tag{30}$$

In the above, the kets (bras) $|E_{s\pm}^{\kappa}\rangle$ apply to the case where H_{SO} is included with H_R. If H_{SO} is included with H_{JT},$|n, E_{s\pm}^{\kappa}\rangle$ should be replaced by the spin-vibronic eigenket $|n, \tilde{E}_{s\pm}^{\kappa}, \Sigma\rangle$. In the next section, we detail how to obtain the derivatives of the rotational constant tensor components. In section S1 of the Supporting Information, we provide the symmetry properties for the derivatives of the rotational tensor. In section S2 of the Supporting Information, we provide some equivalent definitions of h_1 and h_2 in terms of the Cartesian basis, which will be useful to those who choose to work in these coordinates. The calculation of the values of the h_i is discussed in more detail in section S3 of the Supporting Information.

2.4. Computational Procedures. The components of the electronic state can be chosen to transform as distinct representation, in some Abelian subgroup ($\mathcal{g}$) of the molecular symmetry group ($\mathcal{G}$). The two states are labeled here as Γ_1 and Γ_2. Table 2 lists the transformation properties of components of the degenerate state in the Abelian subgroup for C_5H_5, NO_3, and CH_3O. The adiabatic potential energy surfaces (PES) of Γ_1 and Γ_2 are determined using equation of motion-coupled cluster singles and doubles theory (EOMIP-CCSD) using the CFOUR package. The reference state for these EOMIP-CCSD calculations is taken to be the corresponding anion. The adiabatic, electronic eigenfunctions, ψ_{Γ_1} and ψ_{Γ_2}, which are calculated, are related to the previously defined basis functions $|\Lambda = \pm 1\rangle$ by

Table 2. Transformation Properties of Components of the Degenerate State in the Abelian Subgroup

molecule	$\mathcal{G}$	$\mathcal{g}$	state	components in Abelian subgroup
C_5H_5	D_{5h}	C_{2v}	$\tilde{X}^2E_1''$	$^2A_2$ and $^2B_1$
NO_3	D_{3h}	C_{2v}	$\tilde{A}^2E_1''$	$^2A_2$ and $^2B_1$
CH_3O	C_{3v}	C_s	$\tilde{X}^2E$	$^2A'$ and $^2A''$

$$|\Lambda = \pm 1\rangle = \frac{1}{\sqrt{2}}(|\psi_{\Gamma_1}\rangle \pm i|\psi_{\Gamma_2}\rangle) \tag{31}$$

The various coefficients of the Jahn−Teller Hamiltonian (eq 19) are obtainable in terms of first and second derivatives of the *adiabatic* PES of Γ_1 and Γ_2, in terms of dimensionless normal coordinates. Of course a quantum chemistry package produces derivatives with respect to the Cartesian displacements of the atoms, but the transformation of these to dimensionless normal coordinates is straightforward.[29] In the work discussed here, done in the rectilinear normal coordinate representation, each degenerate normal mode ($q_i \; \forall \, f+1 \le i \le f+g$) has two components, q_{ia} and q_{ib}, which are chosen such that q_{ia} transforms as the totally symmetric representation of the Abelian subgroup ($\mathcal{g}$). The first and second derivatives of the adiabatic PES of Γ_k, where k = 1 or 2, with respect to dimensionless normal coordinate, q_i (or q_{ia} and q_{ib} for a degenerate mode), are

$$f_i^{\Gamma_k} = \left.\frac{\partial E_k}{\partial q_i}\right|_{q_0} \tag{32}$$

$$f_{ij}^{\Gamma_k} = \left.\frac{\partial^2 E_k}{\partial q_i \partial q_j}\right|_{q_0} \tag{33}$$

where E_k is the energy of the kth adiabatic state. The relationship between the Cartesian components and the cylindrical representation used in eq 19 is given by

$$q_{i\pm} = q_{ia} \pm i q_{ib} \tag{34}$$

For a JT system, the derivatives of the diabatic PES with respect to totally symmetric (in $\mathcal{g}$) normal coordinate, q_{ia}, are identical to those of the adiabatic PES of Γ_1 and Γ_2.[16,30] Therefore, the parameters in Table 1, defined in terms of the matrix elements of $\hat{\mathcal{H}}_e$, are related to linear and quadratic force constants (f) involving nondegenerate modes ($q_i \; \forall \; 1 \le i \le f$) and the totally symmetric component of degenerate modes (q_{ia} $\forall \; f+1 \le i \le f+g$) as

$$k_i = f_{ia}^{\Gamma_1} = -f_{ia}^{\Gamma_2} \tag{35}$$

$$d_i = f_i^{\Gamma_1} = f_i^{\Gamma_2} \tag{36}$$

DOI: 10.1021/acs.jpca.9b03360
J. Phys. Chem. A 2019, 123, 4990−5004

$$\lambda_i = \frac{1}{2}(f_{iaia}^{\Gamma_1} + f_{iaia}^{\Gamma_2}) \tag{37}$$

$$\lambda_i' = f_{ii}^{\Gamma_1} = f_{ii}^{\Gamma_2} \tag{38}$$

$$g_{ii} = \frac{1}{2}(f_{iaia}^{\Gamma_1} - f_{iaia}^{\Gamma_2}) \tag{39}$$

$$b_{ij} = f_{ija}^{\Gamma_1} = -f_{ija}^{\Gamma_2} \tag{40}$$

$$g_{ij} = \frac{1}{2}(f_{iaja}^{\Gamma_1} - f_{iaja}^{\Gamma_2}) \tag{41}$$

These relations are obtained using eq 31 and eq 34 together with relatively simple symmetry relations and are consistent with Table 1 of ref 16. Tables giving values of these parameters for C_5H_5, CH_3O, and NO_3 are provided in the Supporting Information. Using these values, we can now solve the Hamiltonian in eq 17. One needs to emphasize here that while we use EOMIP-CCSD to obtain these parameters, any quantum chemical method can be useful for this calculation, as long as it provides a proper treatment of the degenerate states and satisfies the associated symmetry properties.

To obtain numerical values for the rotational tensor components, we note that the rotational tensor, $\boldsymbol{B}$ (in cm^{-1}), is related to the inertial tensor ($\boldsymbol{I}$) by

$$\boldsymbol{B} = \frac{h}{8\pi^2 c}\boldsymbol{I}^{-1} \tag{42}$$

where c is the speed of light and $\boldsymbol{I}$ is written in the molecular frame (x, y, z) and has the form

$$\boldsymbol{I} = \begin{pmatrix} \sum_i (y_i^2 + z_i^2)m_i & -\sum x_i y_i m_i & -\sum x_i z_i m_i \\ -\sum y_i x_i m_i & \sum_i (x_i^2 + z_i^2)m_i & -\sum y_i z_i m_i \\ -\sum z_i x_i m_i & -\sum z_i y_i m_i & \sum_i (x_i^2 + y_i^2)m_i \end{pmatrix} \tag{43}$$

The sum is taken over all atoms of the molecule with x_i, y_i, z_i being the Cartesian coordinates of each atom. Derivatives of the inertial tensor with respect to dimensionless normal coordinates are calculated numerically using finite differences. The first and second derivatives of the rotational tensor are calculated using the derivative of inertial tensor as follows:

$$\frac{\partial \boldsymbol{B}}{\partial q_i} = -\frac{h}{8\pi^2 c}\boldsymbol{I}^{-1}\cdot\frac{\partial \boldsymbol{I}}{\partial q_i}\cdot\boldsymbol{I}^{-1} \tag{44a}$$

$$\frac{\partial^2 \boldsymbol{B}}{\partial q_i \partial q_j} = \frac{h}{8\pi^2 c}\left[\boldsymbol{I}^{-1}\frac{\partial \boldsymbol{I}}{\partial q_i}\boldsymbol{I}^{-1}\frac{\partial \boldsymbol{I}}{\partial q_j}\boldsymbol{I}^{-1} - \boldsymbol{I}^{-1}\frac{\partial^2 \boldsymbol{I}}{\partial q_i \partial q_j}\boldsymbol{I}^{-1} + \boldsymbol{I}^{-1}\frac{\partial \boldsymbol{I}}{\partial q_j}\boldsymbol{I}^{-1}\frac{\partial \boldsymbol{I}}{\partial q_i}\boldsymbol{I}^{-1}\right] \tag{44b}$$

These equations are used to calculate the derivatives in Cartesian coordinates, which are then transformed to cylindrical coordinates. The methodology for converting them to cylindrical coordinates and complete set of values for the derivatives of rotational and inertial tensor for C_5H_5, NO_3, and CH_3O are included in the Supporting Information.

3. RESULTS

To benchmark our theoretical calculations, we have selected three radicals, cyclopentadienyl (Cp), C_5H_5; methoxy, CH_3O; and nitrate, NO_3; each of which have been extensively studied experimentally. All three contain a relatively small number of atoms, so they should be amenable to quantum chemistry calculations of relatively high quality. These same characteristics are ideal for spectroscopic study, and experimental values of h_i of relatively high precision are available for them.

As eqs 27−30 show, the rotational distortion parameters h_1 and h_2 depend upon the derivatives of the components of the rotational tensor, whose values are in the Supporting Information. The h_i parameters also critically depend upon the spin-vibronic eigenfunctions. These eigenfunctions, specifically the coefficients in the basis functions expansions of eqs 22 and 23, are obtained by diagonalizing the Hamiltonian matrix, H_V ($+H_{SO}$), which in turn depends upon the JT (and spin) parameters contained in the spin-vibronic Hamiltonian of eqs 19a, 19b, 19c, and 20. As noted before, we use our SOCJT2 software to obtain these eigenvalues and functions.

The parameters in H_{JT} and H_{SO} can be obtained by one of two general ways. As explained in Section 2.4, they can be determined directly from the derivatives (see Table 1) of the calculated electronic PES. The second approach is to fit these parameters to the difference of the spin- vibronic eigenvalues determined spectroscopically. While the spectroscopically fit values are usually of relatively high precision, limitations to the availability of sufficient experimental data often dictate rather severe truncations of the Hamiltonian and correspondingly may introduce some bias into the parameters.[16] Of course all of the terms of the quadratic JT Hamiltonian may readily be determined via quantum chemistry calculations, but those of H_{SO} may not be available in some computation packages.

3.1. Ground $\tilde{X}^2E_1''$ State of Cyclopentadienyl (Cp), C_5H_5, Radical. Cyclopentadienyl (Cp), C_5H_5, is a relatively small hydrocarbon radical that has been studied extensively, both experimentally and computationally. Cp is a good candidate for studying JT effects in that it has five equivalent C and H atoms and belongs to the symmetry group, D_{5h}. Its ground electronic $\tilde{X}$ state is doubly degenerate ($^2E_1''$) and possesses several JT-active vibrations. Group theoretically, e'_2 vibrations are linearly JT-active only, whereas e'_1 vibrations are quadratically Jahn−Teller active only. This fact is convenient for determining h_1' and h_1'', as h_1' only has contributions from modes which are linearly JT-active, whereas h_1'' only has contributions from quadratically active Jahn−Teller modes. In addition, Cp has a plane of symmetry, so h_2' vanishes as is shown subsequently.

The spectroscopy of Cp has been studied for more than 50 years, with its electron paramagnetic resonance spectrum (EPR) observed in 1963[31] and electronic absorption spectrum first observed[32] in 1970. Subsequently, photodetachment (PD), and rotationally and/or vibrationally resolved laser-induced fluorescence (LIF), and laser excited dispersed fluorescence (LEDF) spectroscopic methods have all been utilized to probe geometric distortions from the predicted equilibrium structure with D_{5h} symmetry. Recent spectroscopic experiments at low temperature include jet-cooled LIF,[33,34] LEDF,[35] PD[36] of $C_5H_5^-$, and mid-IR absorption of Cp in He droplets.[37] These papers cite the numerous experiments performed in the intervening years.

DOI: 10.1021/acs.jpca.9b03360
J. Phys. Chem. A 2019, 123, 4990−5004

Early quantum chemistry calculations on Cp appeared in 1956(!)[38] and 1960,[39] and numerous calculations followed thereafter. The most recent calculations relevant to the JT effect in Cp were published[36,40] in the early 21st Century and cite most of the quantum chemistry calculations in the intervening years.

Following the procedures outlined in Section 2.4, quantum chemistry calculations were carried out on Cp with the EOMIP-CCSD method using the ground electronic state of the anion as the reference. Table S5 of the Supporting Information list the symmetries and harmonic vibrational frequencies resulting from the calculation. It tabulates the linear and quadratic JT coupling constants in terms of k_i and g_{ii} which are contained in the Hamiltonian in eqs 19a, 19b, and 19c, and it also provides the conventional JT experimental parameters D_i and K_i, which are used as input to SOCJT2. Table S6 provides the bilinear and cross-quadratic JT coupling constants.

Using SOCJT2 to solve the complete vibronic Hamiltonian for C_5H_5 is impossible because of the huge size basis set that would be needed for the computation given the large number of linear and quadratic JT-active vibrational modes. To alleviate this problem, we ignore the cross quadratic coupling between the linear (e'_2) and quadratic (e'_1) modes. This allows us to do separate calculations for the four e_2' (ν_8, ν_9, ν_{10} and ν_{11}) and three e_1' modes (ν_5, ν_6 and ν_7). For the e_2'-mode-only calculation, the vibronic basis set is truncated at $v_{max} = 8$ except for ν_8 which is truncated at $v_{max} = 4$. The Lanczos algorithm is run for 1000 iterations to get the converged eigenvalues and eigenvectors. For the e_1' mode only calculation, the vibronic basis set is truncated at $v_{max} = 10$ and the Lanczos algorithm is run for 800 iterations to get the eigenvalues and eigenvectors.

The outputs of SOCJT2 are vibronic eigenenergies and eigenkets. The latter are used to calculate matrix elements of the linear and bilinear combinations of the normal coordinates given in Tables S7 and S8, which as eqs 23 and 28 show, are necessary to calculate values for h_1. These equations also require the derivatives of the components of the rotational tensor. As outlined in Section 2.4, these are obtained from the derivatives of the inertial tensor. The resulting values are tabulated in Tables S9−S16. Tables S17−S18 contain respectively the resulting h_1' values and h_1'' values for the vibronic levels of C_5H_5 with energies less than 2200 cm^{-1}.

The rotationally resolved spectrum of the $\tilde{A}^2A_1''$−$\tilde{X}^2E_1''$ origin transition has been observed and analyzed, yielding an experimental value of $|h_1|$= 211.8(3) MHz for the zero-point level of the Cp $\tilde{X}$ state.[33,34] Referring to Table 3, we see that the calculated value of h_1 is 207.4 MHz. While this agreement is somewhat fortuitous in that it certainly exceeds the expected accuracy of the procedure and quantum chemistry treatment used here, it also tends to affirm the computational method. We also see from Table 3 that, for practical purposes, h_1'' is negligible compared to h_1' for Cp.

Table 3. Calculated and Experimental Values (MHz) of $|h_1|$[a] for the Vibrationless level of the $\tilde{X}^2E_1''$ of C_5H_5

vibrational mode symmetry	h_1'	h_1''
e'_2 (linear JT)	−207.1	0
e_1' (quadratic JT)	0	−0.3
vibronic calculation $\|h_1\|$	207.1	0.3
Watson calculation $\|h_1\|$	247.9	
experimental $\|h_1\|$	211.8(3)	

[a]Note that while relative signs of h_1' and h_2'', as well the contributions to them from individual modes, are determined, their overall sign is not as it depends on an arbitrary phase factor.

In the Introduction we noted that in his early work, Watson introduced an approximate, perturbative formula for computing parameters directly related to the h_i. Those formulas yield the following relations for the h_i

$$h_1 \approx \sum_i \sqrt{2D_i}\,\frac{\partial B_{xx}}{\partial q_{ia}} \tag{45}$$

and

$$h_2 \approx \sum_i \sqrt{2D_i}\,\frac{\partial B_{xz}}{\partial q_{ia}} \tag{46}$$

where i refers to the JT active doubly degenerate normal modes and q_{ia} denotes the totally symmetric component in the Abelian subgroup. Such simple relations are obtainable from eqs 27−30 by assuming only a linear JT interaction parametrized by D_i and treating its effect via perturbation theory.

Table 3 shows that using the Watson formulation we calculate $h_1 = h_1'$ = 247.9 MHz. This is a good estimate for h_1 but, as one might expect, less so than the one from the vibronic calculation. Since we know that the quadratic contribution to the power series expansion of the rotational derivative is negligible, the limitation of the Watson approach for C_5H_5 is likely to be the treatment by perturbation theory.

3.2. Ground $\tilde{X}^2E$ State of Methoxy, CH_3O, Radical. The $\tilde{X}^2E$ state of methoxy radical, CH_3O, is perhaps the most studied example of the JT effect, both theoretically and experimentally. Moreover, it provides an example with significant spin−orbit coupling. With C_{3v} symmetry, methoxy has $3a_1$ and $3e$ vibrations, with the latter being JT active. The $\tilde{X}^2E$ state of methoxy has been characterized experimentally by PD spectra[41,42] from the anion, and by numerous optical techniques: emission,[43] laser paramagnetic resonance (LMR),[44,45] and LIF,[46−50] LEDF,[51] and stimulated emission pumping (SEP),[52−54] via its $\tilde{A}^2A_1$ − $\tilde{X}^2E$ electronic transition. In addition, IR absorption[55] and microwave rotational spectra[56,57] in the $\tilde{X}$ state have been observed. Both h_1 and h_2 values have been measured in the zero-point level of each the $^2E_{1/2}$ and $^2E_{3/2}$ (spin−orbit) components of its $\tilde{X}$ state. The highest precision values of h_1 and h_2 are a result of fits[54] to combined microwave and LIF data.

Methoxy has also been a subject of numerous theoretical studies,[58−64] some of these combining experimental with computational work. However, none has addressed the calculation of h_1 and h_2. Following the approach of Section 2.4, we have performed an EOMIP calculation on methoxy with the anion as the reference state. Table S19 of the Supporting Information lists the symmetric harmonic vibrational frequencies and JT parameters resulting from this calculation. These parameters and the spin−orbit coupling parameters are required as input to SOCJT2. For the spin−orbit coupling, we use the value[42] of $a_{\|}$ = 133 cm^{-1} consistent with the value previously computed and which approximately yields the observed quenched spin−orbit coupling, which was previously measured[54] at 61.495 cm^{-1}. Our calculations show that the bilinear and cross-quadratic couplings for CH_3O are negligible and are not included in the SOCJT2 analysis.

DOI: 10.1021/acs.jpca.9b03360
J. Phys. Chem. A 2019, 123, 4990−5004

For CH_3O, the vibronic calculation included the three modes (ν_4, ν_5 and ν_6) which are JT active. The vibronic basis set is truncated at v_{max} = 10 for all three modes. The SOCJT2 input parameters for CH_3O are given in Table S19. The eigenket output is used to calculate the matrix elements of the normal coordinates that appear in the definitions of the h_i and whose values are given in Table S20. In addition, first and second derivatives of the elements of the rotational tensor are listed in Tables S21−S26. The resulting h_1 and h_2 values for methoxy for vibrational levels up to 2000 cm^{-1} above the zero-point $\tilde{X}$ state level are given in Tables S27 and S28.

In Table 4, we compare the experimental values of h_1 and h_2 with the calculated results. As the table shows, once again there is good agreement between calculated and experimental values of the h_1. Considering the experimental uncertainties (see below) the agreement for h_2 is also good, albeit not as spectacular as that for h_1. The methoxy results tend to confirm the validity of the calculation even when spin orbit coupling is present with a magnitude comparable to JT distortion.

Table 4. Values (MHz) of h_1 and h_2 in the $^2E_{1/2}$ and $^2E_{3/2}$ Spin Components of the Vibrationless Level of the $\tilde{X}^2E$ State of CH_3O

	$\lvert h_1\rvert$		$\lvert h_2\rvert$	
method	$E_{3/2}$	$E_{1/2}$	$E_{3/2}$	$E_{1/2}$
vibronic calculation	72.22[a]	77.61[b]	1208[c]	1301(26)[d]
vibronic calculation (av.)	74.91		1268	
Watson calculation (av.)	86		1587	
experimental	75.45(26)		1331(3)	

[a] $h_1' = -64.58$; $h_1'' = -7.63$. [b] $h_1' = -69.24$; $h_1'' = -8.36$. [c] $h_2' = -1199.2$; $h_2'' = -9.3$. [d] $h_2' = -1315.7$; $h_2'' = -10.2$.

For h_1, it is clear that h_1'' is small compared to h_1'. However, due to the larger magnitude of h_2, the same is more true for h_2'' relative to h_2'. Finally, we note that the vibronic calculation and Watson approximation agree fairly well for h_1, but the more rigorous vibronic calculation agrees significantly better with experiment for h_2.

Before closing the discussion on methoxy, it is worthwhile to note a few points about the comparison between calculated and experimental values. Reference 54 provides a table with the experimental parameters of CH_3O determined with four different combinations of data. Generally speaking, all the parameters are consistent within their statistical errors, which in turn are reflective of the overall size and precision of the respective data sets. It is, however, worth noting that the standard deviation of the h_i among the four sets is 0.50 MHz for h_1 and 53 MHz for h_2. Clearly the statistical error for h_1 and its deviation among sets is comparable, while the deviation for h_2 among data sets is much greater and possibly indicates less reliability for the experimental value of h_2 than its statistical error indicates.

There is another interesting point. Theoretically one would expect h_1 and h_2 to vary modestly between spin components as is indeed shown by the calculated values. Nonetheless, and understandably, the fit to the experimental spectra constrained the h_i values to be equal for both spin components. This possibly contributes to the relatively poor agreement among the h_2 values obtained from different data sets.

3.3. Excited $\tilde{A}^2E''$ State of Nitrate, NO_3, Radical. The three lowest electronic states, $\tilde{X}^2A_2'$, $\tilde{A}^2E''$, and $\tilde{B}^2E'$, of the nitrate radical, NO_3, have long been explored spectroscopically and investigated by quantum chemistry methods. The $\tilde{X}$ and $\tilde{B}$ states have been most studied and considerable interest in them remains. The $\tilde{A}$ state has been less studied, principally because transitions between it and the ground $\tilde{X}$ state are electronically forbidden for electric dipole radiation. Nonetheless, in recent years, weak vibronically allowed and magnetic dipole transitions have been observed by cavity ringdown spectroscopy (CRDS).[65−69] The $\tilde{A}$ state has also been studied experimentally by PD spectroscopy.[70] These experiments have further stimulated interest from quantum chemistry.[66,67,69,71−75]

Our focus here is on the $\tilde{A}$ state, which transforms as E″ in the D_{3h} point group. It has one a_1', one a_2'', and two e′ vibrational modes, with the latter two being JT-active. In addition, PJT coupling exists in first or second order between all three states, with $\tilde{X}$−$\tilde{B}$ linear coupling being particularly strong and ultimately responsible for the great complexity of the NO_3 molecule.

Rotationally resolved spectra have been observed for several bands of the jet-cooled $\tilde{A}$−$\tilde{X}$ CRDS spectrum. None of the observed bands show definitive evidence of the effect of h_1, and an upper limit for $|h_1|$ of less than 75 MHz for the zero-point level can be established as is reflected in Table 5. (No values of h_1 have been reported for the $\tilde{B}$ state of NO_3, although it is also JT-active, due at least in part to an extremely complicated $\tilde{B}$−$\tilde{X}$ spectrum. Of course h_2 = 0 in both states due to planarity.)

Table 5. Values (MHz) of h_1 for the Vibrationless Level of the $\tilde{A}^2E$ State of NO_3

	eigenfunction source	
	electronic structure calculation	analysis of vibronic spectrum[a]
h_1'[b]	60.5	−190
h_1''[b]	−8.0	24
$\lvert h_1'\rvert$[b]	52.5	166
$h_1' = h_1$[c]	467	385
$\lvert h_1\rvert$(exp)	≤75[d]	

[a] Reference 69. [b] Vibronic calculation. [c] Watson calculation. [d] Experimental upper limit for h_1 determined for the 2^1 e′ vibronic level of the $\tilde{A}$ state, which, to the level of theory in the calculation, is the same as the vibrationless level.

For NO_3, the vibronic calculation included three modes: ν_1, which is a nondegenerate mode, and ν_3 and ν_4, which are JT-active degenerate modes. The vibronic basis set is truncated at v_{max} = 10 for all three modes. The Lanczos algorithm is run for 1200 iterations to get the converged eigenvalues and eigenvectors. Nonzero bilinear coupling between ν_1 and the degenerate modes is also included in the calculation.

Table 5 shows the values of h_1 for the zero-point level calculated from the vibronic eigenkets using the same procedures as previously described for C_5H_5 and CH_3O. Corresponding values for JT coupling parameters, matrix elements of the normal coordinates, values of rotational tensor component derivatives, and h_1 values for higher levels are given in Tables S29−S37 of the Supporting Information. As one can see from Table 5, the calculated value of h_1 is somewhat smaller than the experimentally observed upper limit and is therefore consistent with it. One can also note that, for NO_3, the calculated value of h_1'' is not very small compared to h_1', in contrast to both C_5H_5 and CH_3O. This is clearly consistent with the strong JT effect in NO_3. Furthermore, we note the calculation of h_1 by the Watson method is clearly inconsistent

DOI: 10.1021/acs.jpca.9b03360
J. Phys. Chem. A 2019, 123, 4990−5004

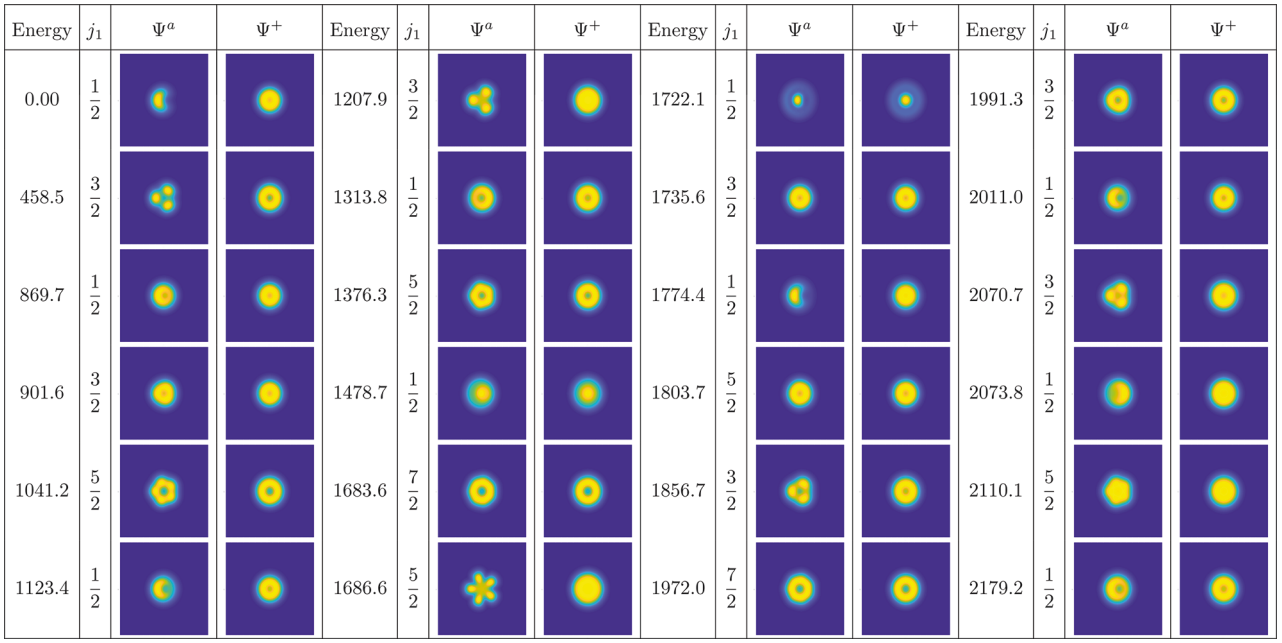

Figure 1. Plots of vibronic density, $|\Psi^a|^2$ and $|\Psi^+|^2$, for the normal mode polar coordinates ρ_9 and θ_9 for the lowest vibronic levels of C_5H_5. The two densities are integrated over the electronic component and other vibrational components as described in section S5.1 of the Supporting Information. The ρ_9 is the distance from origin and varies from 0 to 10 at the corner in reduced (dimensionless) normal coordinates, which are related to the standard mass-weighted normal coordinates as $Q_i = \frac{10.9726694787\rho_i}{\sqrt{\omega_i}}$, where Q_i is in $(\text{amu})^{1/2}$bohr and ω is the harmonic frequency of the mode in cm^{-1} (for more detail see footnote 53 of ref 30). θ_9 is the angle with the x-axis in the anticlockwise direction and varies from 0 to 2π. The color scale indicates the magnitude of the density, with yellow the maximum. The individual plots are labeled by vibronic eigenenergy and its value of j_1.

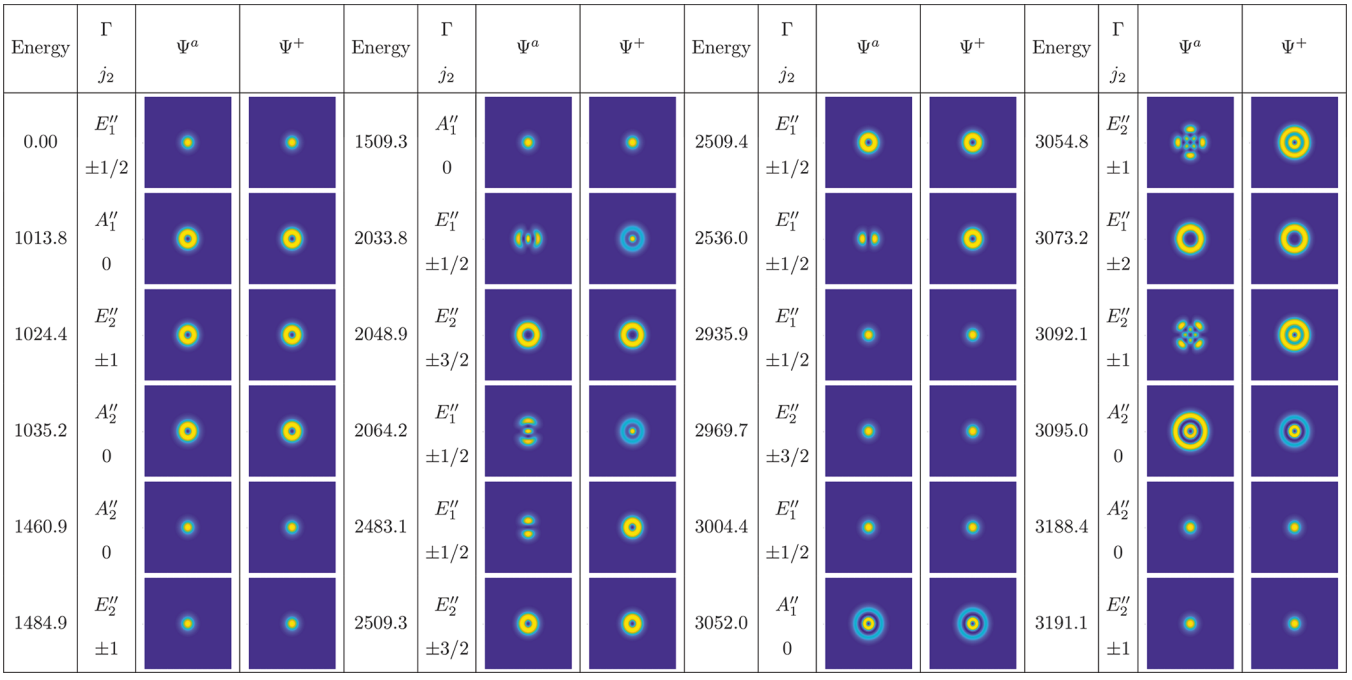

Figure 2. Plots of vibronic density, $|\Psi^a|^2$ and $|\Psi^+|^2$, for the normal mode polar coordinates ρ_7 and θ_7 for the lowest vibronic levels of C_5H_5. The rest of the information is the same as given in the caption for Figure 1. The individual plots are labeled by vibronic eigenenergy and its value of j_2.

with the experimental result as well as the vibronic calculation, reflecting a failure of first-order perturbation theory in this case where the JT coupling is extremely strong.

Table 5 makes one other comparison. As discussed in the Introduction, the JT parameters can also be extracted from an analysis of the experimental vibronic spectra, which as Table S29 shows, are (considerably) larger than the calculated ones. The value of h_1 calculated with these parameters is therefore larger, as seen in Table 5, and indeed is significantly larger than the experimental upper limit for h_1, which further suggests that the experimentally inferred potential is flawed as has been discussed previously.[16] Indeed, a virtue of h_1 and h_2 is that they

DOI: 10.1021/acs.jpca.9b03360
J. Phys. Chem. A 2019, 123, 4990−5004

allow the benchmarking of low-order terms in the JT expansion calculated by theory. Should higher order terms, e.g., h_i''', be required to make calculations and experiment agree, it is indicative that a higher order JT expansion is necessary.

4. DISCUSSION

We have derived a method for predicting h_1 values from vibronic eigenfunctions based on the results of quantum chemistry calculations, and we have demonstrated that this approach yields predictions in good agreement with experimental values for representative examples. It is useful to apply our computational approach to look more generally at the characteristics of the h_i distortion parameters.

The symmetry properties of the vibronic eigenfunctions are important for the values of the h_i and indeed many other molecular parameters. One symmetry property that has long been known is that h_2 vanishes for a planar molecule. This property derives from the fact that h_2 is proportional to a rotational tensor component that is inversely proportional to the z displacement of the nuclei, which transforms antisymmetrically with respect to reflection in the plane. However, the direct product of the vibronic eigenkets always transforms symmetrically, and hence the vibronic matrix elements in eqs 29 and 30 must vanish through first order. This result has been previously obtained but based on consideration of the symmetry of H_{JT} alone. If spin−orbit coupling is considered, the spin-double-group irreducible representations are still symmetric for the bra-ket direct product, while the rotational tensor components still transform antisymmetrically. Hence, h_2 vanishes for planar molecules, whether or not spin−orbit coupling is considered.

More information about the h_i can be obtained for particular molecules, and the Cp radical is a particularly convenient example to consider. Since it is planar, h_2 vanishes. The Cp radical has vibrational modes of one symmetry, e'_2, that have a linear-only JT effect and others, e'_1, that have a quadratic-only JT effect. The interaction between modes of these two symmetries is negligible and indeed has been omitted from our calculations on Cp as mentioned earlier. The values of h'_1 that we have calculated are given in Table S17 for e'_2 levels and h''_1 in Table S18 for e'_1 levels. As noted from those tables, all values of h''_1 and h'_1 vanish for the e'_2 and e'_1 modes, respectively. This follows from the fact that the linear and quadratic JT effects vanish for e'_1 and e'_2 modes respectively, and hence h'_1 and h''_1 must correspondingly vanish. However, what we found surprising is that in Table S17 many other values of h'_1 also vanish for e'_2 vibrational modes as do values for h''_1 in Table S18 for e'_1 vibrational modes.

To investigate the situation in more detail, we have plotted vibronic densities of the Cp radical in Figures 1 and 2. The method used to calculate the densities follows from that reported by Ichino et al.,[36] and details of our implementation are given in the Supporting Information. These plots are constructed using the same vibronic eigenfunctions that were used to calculate the h_i values for each molecule. The plots in the figures are for the normal mode of the given molecule that best illustrates the characteristics of the vibronic density, usually the one that has the strongest linear JT interaction.

To understand the vibronic density plots shown in the figures for Cp, it is useful to introduce the quantum number, j_k, which is a function of l and Λ, with its detailed form depending on the molecule's symmetry group and the irreducible representations according to which the electronic $\psi^{\epsilon}_{\pm|\Lambda|}$ and vibrational $\psi_{v,l}$ wave functions transform. Child and Longuet-Higgins[17] first used j_1 (therein called just j), and its definition was extended to j_k in the review by Barckholtz and Miller.[4] As shown therein, j_k is a good quantum number for Ψ^{SV} if there is only a single order of JT interaction; i.e., for a linear JT interaction, $k = 1$, for a quadratic interaction, $k = 2$, etc. Since Λ and l can assume both positive and negative values, j can also have positive and negative values, and we denote the corresponding eigenfunctions as $\Psi^{SV}(\pm j_k)$, which can be taken as the two components of the degenerate vibronic eigenvalue. Generically, these eigenfunctions are referred to as $\Psi^{\pm}$ regardless of whether j_k is a good quantum number.

Of course, for a given j_k, a linear combination of $\Psi^{SV}(\pm j_k)$ remains an eigenfunction of the vibronic Hamiltonian. However, if we want also to diagonalize the h_i operators to first order, we need to take a form like

$$\Psi^{a}(|j|) = \frac{1}{\sqrt{2}}[\Psi^{SV}(j) + \Psi^{SV}(-j)] \tag{47}$$

$$\Psi^{b}(|j|) = \frac{i}{\sqrt{2}}[\Psi^{SV}(-j) - \Psi^{SV}(j)] \tag{48}$$

since the h_i are defined in terms of matrix elements *between* the degenerate components $\Psi^{SV}(j)$ and $\Psi^{SV}(-j)$.

In the Supporting Information, we show that for these eigenfunctions the vibronic density can be written

$$|\Psi^{a/b}(|j|)|^2 = \frac{1}{2}\int [|\Psi^{SV}(j)|^2 + |\Psi^{SV}(-j)|^2 \pm \Psi^{SV*}(j)\Psi^{SV}(-j) \pm \Psi^{SV*}(-j)\Psi^{SV}(j)]\, d\epsilon = \mathcal{F}^k_0\mathcal{G}^k_0(\rho) \pm \mathcal{F}^k_1(\theta)\mathcal{G}^k_1(\rho) \tag{49}$$

The $\mathcal{G}^k_0(\rho)$ and $\mathcal{G}^k_1(\rho)$ are functions only of ρ and consist of sums over products of the associated Leguerre polynomials and the mixing coefficients in the vibronic eigenfunction, which are outputs of SOCJT2. Correspondingly $\mathcal{F}^k_0(\theta)$ and $\mathcal{F}^k_1(\theta)$ are functions of θ only.

In Figure 1 we have plotted $|\Psi^a|^2$ and $|\Psi^+|^2$ for a number of the lower eigenvalues of the e'_2 ν_9 vibration of Cp, which is JT active only for a linear JT interaction, and hence, j_1 is a good quantum number. The plots of $|\Psi^a|^2$ and $|\Psi^+|^2$ are stunning in terms of variety, complexity, and, in many cases, high symmetry. An examination of the $|\Psi^a|^2$ plots shows that they contain axes of rotation, from one to many-fold. Figure 1 shows one symmetry axis for $j = \frac{1}{2}$, 3 axes for $j = \frac{3}{2}$ levels, 5 axes for $j = \frac{5}{2}$ and so on, which must be attributable to $\mathcal{F}^k_1(\theta)$. For any of the e'_2 modes of the ground state of Cp, we show in the Supporting Information that $\mathcal{F}^1_1(\theta) = \cos(2j_1)$, which is consistent with the plots of $|\Psi^a(|j|)|^2$. However, $\mathcal{F}^k_0(\theta)$ has no θ dependence, which explains the lack of structure in the plots of $|\Psi^+|^2$. Nonetheless the existence of both $\mathcal{F}^k_0\mathcal{G}^k_0(\rho)$ and $\mathcal{F}^k_1(\theta)\mathcal{G}^k_1(\rho)$ are important since the plots of $|\Psi^a(|j|)|^2$ are a sum or difference of them. If there is no JT-effect, then the sums involving $C^{\pm}_{v,l}$ reduce to a single term of unity and $\mathcal{G}^k_1(\rho)$ vanishes making the vibronic density independent of θ.

A molecule with a 3-fold or greater proper or improper symmetry axis must be a symmetric (or spherical) top. The converse of this is that a molecule with less than a 3-fold axis is an asymmetric top. The geometry of the molecule, and hence

DOI: 10.1021/acs.jpca.9b03360
J. Phys. Chem. A 2019, 123, 4990−5004

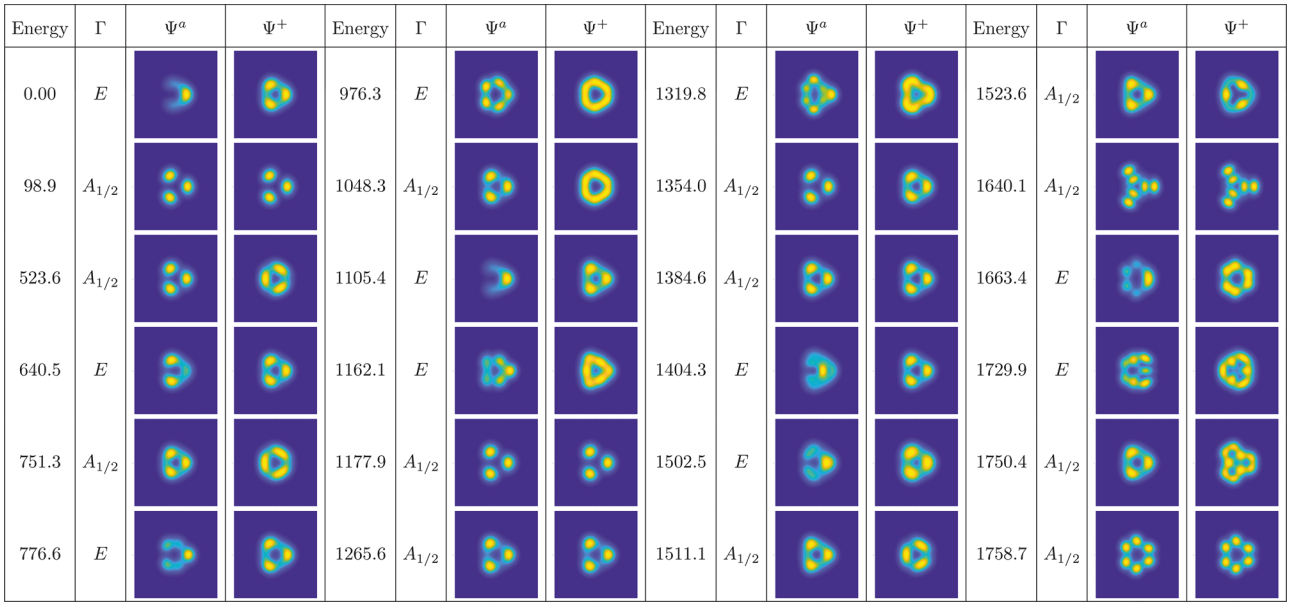

Figure 3. Plots of vibronic density, $|\Psi^a|^2$ and $|\Psi^+|^2$, for the normal mode polar coordinates ρ_3 and θ_3 for the lowest vibronic levels of NO_3. The rest of the information is the same as given in the caption for Figure 1.

its symmetry, is usually determined by the equilibrium positions of the nuclei as defined by expectation values over the electronic eigenfunction. This definition can be extended to include distortions from vibronic coupling, by defining the molecule's inertial tensor to be determined by its expectation value over the vibronic eigenfunction. If that symmetry is 3-fold or greater, the molecule rotationally behaves like a symmetric top. (The statement assumes that the vibrational motion is sufficiently rapid to average the molecular rotations over a vibrational period. If the vibrational motion is not sufficiently rapid, one must correct this picture by taking into account rotation−vibration coupling between different vibronic levels.) From the form of $\mathcal{F}_1^k(\theta)$, the only value of j_1 that has less than a 3-fold axis is $j_1 = \frac{1}{2}$. Hence $j_1 = \frac{1}{2}$ levels will be the only ones to distort from the symmetric top geometry of the non-JT-perturbed configuration, and therefore, only those vibronic states have nonvanishing values of h_1. Another consistent, but less physical, argument is that h_1 must vanish, except for $j = \pm\left|\frac{1}{2}\right|$ levels, is to note that h_1 contains the matrix element of the normal coordinate which has a selection rule of $\Delta l = \pm 1$. To have a nonzero h_1 within a degenerate vibronic state, the values of j connected by the matrix must be equal in magnitude and opposite in sign. Only the values of $j = \pm\frac{1}{2}$ satisfy this criterion, and thereby, we observe the many zero values of h_1' in Table S17.

While Figure 1 is very informative, it is important to remember that so far we have focused on the e'_2 vibrational levels of Cp which show only a linear JT effect. Figure 2 shows comparable vibronic density plots for the e_1' ν_7 mode which is only quadratically JT active. For these levels, j_2 becomes the good quantum number, and we see from the Supporting Information that $\mathcal{F}_1^2(\theta) = \cos(4j_2)$. As expected, the plots of Figure 2 show angular dependence consistent with $\mathcal{F}_1^2(\theta)$. The figure also shows that j_2 takes on both half odd integer and integer values. Only the former states show vibronic densities with less than a 3-fold axis. While there are a number of degenerate e vibronic states with integer j_2, the vibronic densities are all of 3-fold or higher symmetry and should be symmetric tops. This result is confirmed in Table S18, which shows that h_1 vanishes for these states, even if they are of e symmetry.

The plots in Figures 1 and 2 for Cp allow us to make some general observations about the vibronic density $|\Psi^a|^2$. It is important to note that the density is the sum or difference between two terms. The first one of these is $\mathcal{F}_0^k(\theta)\mathcal{G}_0^k(\rho)$, which is independent of θ so long as j_k is a good quantum number. The second of these, $\mathcal{F}_1^k(\theta)\mathcal{G}_1^k(\rho)$, depends on a cosine function of θ. However, this latter term vanishes if there is no JT effect and correspondingly is much smaller than the former for small JT coupling but increases at the expense of the former as the coupling grows.

Overall the vibronic density serves as a powerful tool to identify the characteristics of a particular eigenstate. If the density has 3-fold or higher symmetry, the state behaves as a symmetric top and the h_i vanish. For either a linear-only or quadratic-only JT effect the j_k of a given quantum state can be assigned by noting the characteristic patterns of $\cos(2j_1\theta)$ or $\cos(2j_2\theta)$ in the plots. This can be used to definitively identify a particular eigenstate in a region of dense energy level structure. Moreover the contribution of a particular normal mode can be readily ascertained qualitatively by the relative magnitude of the deviation of the density plot from cylindrical symmetry in the coordinate space (ρ_i,θ_i) of the JT-active normal mode, e.g., for the e_2' vibration modes, $i = 8-11$, of Cp.

Many molecules also have a significant linear and quadratic effect in the same mode, and one of these is NO_3, whose h_1 values are given in Table S28 with a corresponding plot of the density of the vibronic eigenfunctions in Figure 3. Of course, j is no longer a good quantum number for NO_3, and the vibronic eigenfunctions contain multiple, but not unrestricted, values of j. However, the D_{3h} symmetry designations of e′ or a′ (a_1' or a_2') still apply and the eigenfunctions for e levels contain only basis functions, $j = \frac{1}{2} + 3n$. Only e′ levels have $|\Psi^a|^2$ with less than a 3-fold axis and so can support a nonzero

DOI: 10.1021/acs.jpca.9b03360
J. Phys. Chem. A 2019, 123, 4990−5004

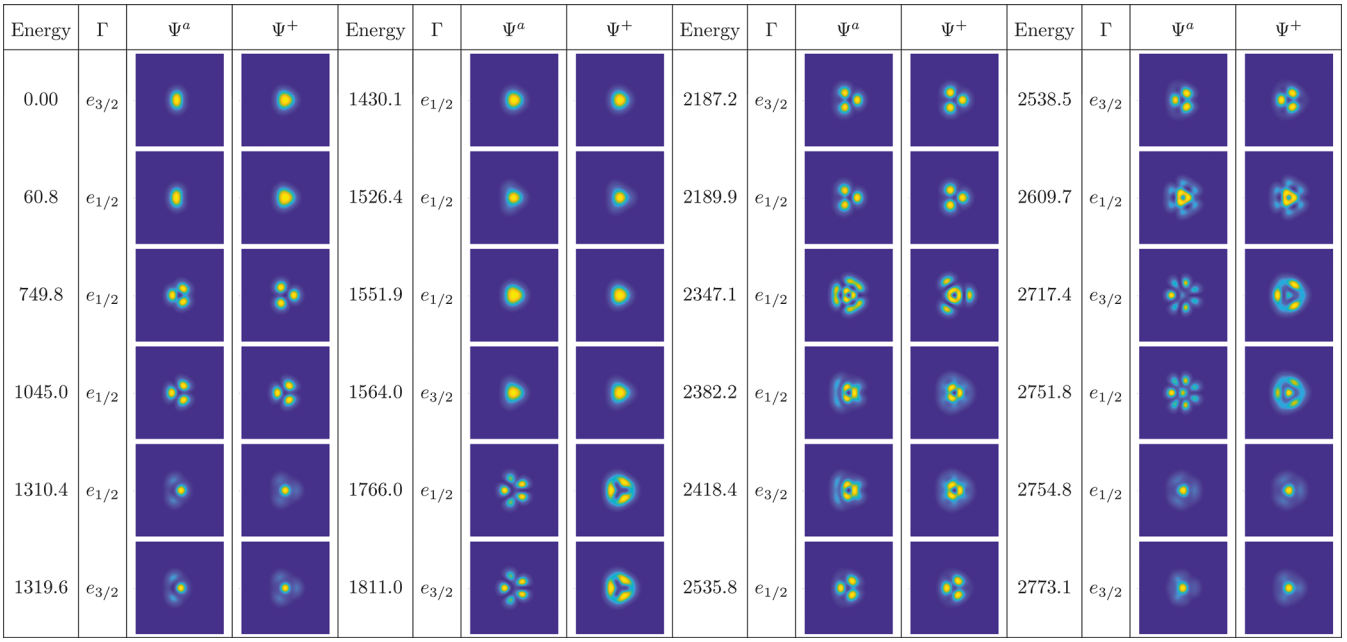

Figure 4. Plots of vibronic density, $|\Psi^a|^2$ and $|\Psi^+|^2$, for the normal mode polar coordinates ρ_6 and θ_6 for the lowest vibronic levels of CH_3O. The rest of the information is the same as given in the caption for Figure 1.

value of h_1, as Table S37 clearly shows. However, for NO_3, unlike Cp, all the degenerate levels have finite values for h_1. We note that $\mathcal{F}_0^1(\theta)$ is no longer θ independent due to cross-terms therein involving different j values which leads to a θ dependence with 3-fold symmetry for $|\Psi^+|^2$ in the plots.

Finally, we turn to Figure 4 for CH_3O which has both linear and quadratic coupling in its e vibrational modes. Correspondingly the plots in Figure 4 for both $|\Psi^a|^2$ and $|\Psi^+|^2$ show structure similar to those for NO_3. Again, the nominally e states alone show less than a 3-fold symmetry axis and support nonzero h_i values. There is additionally a significant spin−orbit coupling in CH_3O that is lacking in NO_3. This leads to spin−orbit pairs of states in Figure 3 with structure that is indistinguishable at the resolution of the plots, even though small differences in the h_i values are calculated for them.

5. CONCLUSIONS

The importance of CIs in chemistry is now widely recognized despite the challenges they pose for characterization experimentally or via electronic structure calculations. While CIs of electronic PESs are ubiquitous, those associated with the JT effect are the ones most extensively characterized experimentally. The rotational distortion parameters, h_1 and h_2, are examples of the molecular parameters that can be measured accurately by high resolution spectroscopy and are quite sensitive to the PES containing the JT induced CI.

We have formulated the basic theory necessary to relate measured h_1 and h_2 values to those derived from a quantum chemistry calculation of the PES. On the basis of this theory, we have developed computational technology to obtain numerical values for h_1 and h_2, which is easily extended to the computation of other molecular parameters of JT-active systems.

This technology enables computation of values for the h_1 and h_2 parameters of the JT-active $\tilde{X}^2E_1''$ state of C_5H_5, the $\tilde{X}^2E$ state of CH_3O, and the $\tilde{A}^2E''$ state of NO_3. Excellent agreement between the calculated and observed values of the h_i parameters are obtained for C_5H_5 and CH_3O. In the case of NO_3, the calculated value of h_1 is just below its experimentally measured upper limit.

These computational techniques can be applied to determine general properties of the h_1 and h_2 parameters. These parameters can exhibit vanishing values for particular vibronic levels even if a substantial JT effect and corresponding geometric distortion is present. If the vibronic density shows a 3-fold or higher rotational symmetry axis, the h_i parameters vanish in that state. However, if the vibronic density has less than 3-fold symmetry its magnitude for a particular mode is not directly correlated with that state's observed values of h_1 and h_2 since they reflect the distortion from all modes. Nonetheless, the vibronic density plots do readily reflect whether the JT interaction is linear, quadratic, or both.

■ ASSOCIATED CONTENT

Supporting Information

The Supporting Information is available free of charge on the ACS Publications website at DOI: 10.1021/acs.jpca.9b03360.

$h_1 - h_2$ calculations and results (PDF)

■ AUTHOR INFORMATION

Corresponding Authors

*(K.S.) E-mail: sharma.754@osu.edu.
*(T.A.M.) E-mail: tamiller@chemistry.ohio-state.edu.

ORCID

Terry A. Miller: 0000-0003-0731-8006
John F. Stanton: 0000-0003-2345-9781

Present Address

¶Department of Chemistry, University of California, Berkeley, CA 94720

Notes

The authors declare no competing financial interest.

DOI: 10.1021/acs.jpca.9b03360
J. Phys. Chem. A 2019, 123, 4990−5004

■ ACKNOWLEDGMENTS

J.F.S. acknowledges the support of this work by the National Science Foundation via Grant CHE 1664325. KS gratefully acknowledges a Terry A. Miller Postdoctoral Fellowship from The Ohio State University. T.A.M. acknowledges support for S.G. via a Henry and Camille Dreyfus Foundation Senior Scientist Mentor Program Award for Undergraduate Research and support from the Ohio Supercomputer via Project PAS0540. We also gratefully acknowledge contributions to this work by Henry Tran in its early stages.

■ REFERENCES

(1) Herzberg, G.; Longuet-Higgins, H. Intersection of potential energy surfaces in polyatomic molecules. *Discuss. Faraday Soc.* **1963**, *35*, 77−82.
(2) Mead, C. A.; Truhlar, D. G. On the determination of Born−Oppenheimer nuclear motion wave functions including complications due to conical intersections and identical nuclei. *J. Chem. Phys.* **1979**, *70*, 2284−2296.
(3) Yarkony, D. R. Diabolical conical intersections. *Rev. Mod. Phys.* **1996**, *68*, 985.
(4) Barckholtz, T. A.; Miller, T. A. Quantitative insights about molecules exhibiting Jahn-Teller and related effects. *Int. Rev. Phys. Chem.* **1998**, *17*, 435−524.
(5) Barckholtz, T. A.; Miller, T. A. The calculation of spectroscopic Jahn-Teller parameters by *ab initio* methods. *J. Phys. Chem. A* **1999**, *103*, 2321−2336.
(6) Jahn, H. A.; Teller, E. Stability of polyatomic molecules in degenerate electronic states-I−Orbital degeneracy. *Proc. R. Soc. London, A* **1937**, *161*, 220−235.
(7) Levine, B. G.; Martínez, T. J. Isomerization through conical intersections. *Annu. Rev. Phys. Chem.* **2007**, *58*, 613−634.
(8) Levine, B. G.; Coe, J. D.; Martínez, T. J. Optimizing conical intersections without derivative coupling vectors: Application to multistate multireference second-order perturbation theory (MS-CASPT2). *J. Phys. Chem. B* **2008**, *112*, 405−413.
(9) Wörner, H. J.; Merkt, F. Jahn−Teller effects in molecular cations studied by photoelectron spectroscopy and group theory. *Angew. Chem., Int. Ed.* **2009**, *48*, 6404−6424.
(10) Signorell, R.; Merkt, F. PFI-ZEKE photoelectron spectra of the methane cation and the dynamic Jahn−Teller effect. *Faraday Discuss.* **2000**, *115*, 205−228.
(11) Bersuker, I. B. Modern aspects of the Jahn- Teller effect theory and applications to molecular problems. *Chem. Rev.* **2001**, *101*, 1067−1114.
(12) Monkhorst, H. J. Calculation of properties with the coupled-cluster method. *Int. J. Quantum Chem.* **1977**, *12*, 421−432.
(13) Stanton, J. F.; Bartlett, R. J. The equation of motion coupled-cluster method. A systematic biorthogonal approach to molecular excitation energies, transition probabilities, and excited state properties. *J. Chem. Phys.* **1993**, *98*, 7029−7039.
(14) Stanton, J. F. Coupled-cluster theory, pseudo-Jahn−Teller effects and conical intersections. *J. Chem. Phys.* **2001**, *115*, 10382−10393.
(15) Eisfeld, W.; Morokuma, K. A detailed study on the symmetry breaking and its effect on the potential surface of NO 3. *J. Chem. Phys.* **2000**, *113*, 5587−5597.
(16) Tran, H. K.; Stanton, J. F.; Miller, T. A. Quantifying the effects of higher order coupling terms on fits using a second order Jahn-Teller Hamiltonian. *J. Mol. Spectrosc.* **2018**, *343*, 102−115.
(17) Child, M. S.; Longuet-Higgins, H. C. Studies of the Jahn-Teller effect III. The rotational and vibrational spectra of symmetric-top molecules in electronically degenerate states. *Philos. Trans. R. Soc., A* **1961**, *254*, 259−294.
(18) Child, M. S.; Strauss, H. L. Causes of *l*- type doubling in the $3\rho(E'')$ rydberg state of ammonia. *J. Chem. Phys.* **1965**, *42*, 2283−2292.
(19) Hougen, J. T. Double group considerations, Jahn-Teller induced rovibronic effects, and the nuclear spin-electron spin hyperine Hamiltonian for a molecule of symmetry C_{3v} in an electronic ^{2}E state. *J. Mol. Spectrosc.* **1980**, *81*, 73−92.
(20) Watson, J. K. G. Jahn-Teller and L-uncoupling effects on rotational energy levels of symmetric and spherical top molecules. *J. Mol. Spectrosc.* **1984**, *103*, 125−146.
(21) Herzberg, G.; Lew, H.; Sloan, J. J.; Watson, J. K. G. The electronic emission spectrum of triatomic hydrogen. III. Infrared perpendicular bands near 3600 cm^{-1}. *Can. J. Phys.* **1981**, *59*, 428−440.
(22) Bernath, P. F. *Spectra of atoms and molecules*; Oxford University Press: New York, 2005.
(23) Hirota, E. *High-resolution spectroscopy of transient molecules*; Springer-Verlag: New York, 1985.
(24) Barckholtz, T. A.; Miller, T. A. Quantitative insights about molecules exhibiting Jahn-Teller and related effects. *Int. Rev. Phys. Chem.* **1998**, *17*, 435−524.
(25) Bersuker, I. B. *The Jahn-Teller effect*; Cambridge University Press: Cambridge, U.K., 2006.
(26) Stanton, J. F. On the vibronic level structure in the NO_3 radical. I. The ground electronic state. *J. Chem. Phys.* **2007**, *126*, 134309.
(27) Stakhursky, V. L. *Vibronic structure and rotational spectra of radicals in degenerate electronic state. Case of CH_3O and asymmetrically deuterated isotopomers (CHD_2O and CH_2DO)*. Ph.D. Thesis, The Ohio State University, 2005.
(28) Codd, T. J. Spectroscopic studies of the $\tilde{A}^2E''$ state of NO_3. Ph.D. Thesis, The Ohio State University, 2014.
(29) Boatz, J. A.; Gordon, M. S. Decomposition of normal-coordinate vibrational frequencies. *J. Phys. Chem.* **1989**, *93*, 1819−1826.
(30) Stanton, J. F. On the vibronic level structure in the NO_3 radical. I. The ground electronic state. *J. Chem. Phys.* **2007**, *126*, 134309.
(31) Liebling, G. R.; McConnell, H. M. Study of molecular orbital degeneracy in C_5H_5. *J. Chem. Phys.* **1965**, *42*, 3931−3934.
(32) Engleman, R.; Ramsay, D. A. Electronic absorption spectrum of the cyclopentadienyl radical (C_5H_5) and its deuterated derivatives. *Can. J. Phys.* **1970**, *48*, 964−969.
(33) Yu, L.; Foster, S. C.; Williamson, J. M.; Heaven, M. C.; Miller, T. A. Rotationally resolved electronic spectrum of jet-cooled cyclopentadienyl radical. *J. Phys. Chem.* **1988**, *92*, 4263−4266.
(34) Yu, L.; Williamson, J. M.; Miller, T. A. Rotationally resolved electronic spectrum of jet-cooled deuterated cyclopentadienyl radical. *Chem. Phys. Lett.* **1989**, *162*, 431−436.
(35) Applegate, B. E.; Bezant, A. J.; Miller, T. A. The Jahn-Teller and related effects in the cyclopentadienyl radical, part II: Vibrational analysis of the $\tilde{A}^2A_2'' - \tilde{X}^2E_1''$ electronic transition. *J. Chem. Phys.* **2001**, *114*, 4869−4882.
(36) Ichino, T.; Wren, S. W.; Vogelhuber, K. M.; Gianola, A. J.; Lineberger, W. C.; Stanton, J. F. The vibronic level structure of the cyclopentadienyl radical. *J. Chem. Phys.* **2008**, *129*, 084310.
(37) Leicht, D.; Kaufmann, M.; Schwaab, G.; Havenith, M. Infrared spectroscopy of the helium solvated cyclopentadienyl radical in the CH stretch region. *J. Chem. Phys.* **2016**, *145*, 074304.
(38) Liehr, A. D. On the stability of cyclobutadiene, cyclopentadienyl radical, and the benzene plus one ion: A comparison of the molecular orbital and valence bond predictions. *Z. Phys. Chem.* **1956**, *9*, 338−354.
(39) Snyder, L. C. Jahn-Teller distortions in cyclobutadiene, cyclopentadienyl radical, and benzene positive and negative Ions. *J. Chem. Phys.* **1960**, *33*, 619−621.
(40) Applegate, B. E.; Miller, T. A.; Barckholtz, T. A. The Jahn-Teller and related effects in the cyclopentadienyl radical, part I: The *ab initio* calculation of spectroscopically observable parameters. *J. Chem. Phys.* **2001**, *114*, 4855−4868.
(41) Nee, M. J.; Osterwalder, A.; Zhou, J.; Neumark, D. M. Slow electron velocity-map imaging photoelectron spectra of the methoxide anion. *J. Chem. Phys.* **2006**, *125*, 014306.

DOI: 10.1021/acs.jpca.9b03360
J. Phys. Chem. A 2019, 123, 4990−5004

(42) Weichman, M. L.; Cheng, L.; Kim, J. B.; Stanton, J. F.; Neumark, D. M. Low-lying vibronic level structure of the ground state of the methoxy radical: Slow electron velocity-map imaging (SEVI) spectra and Köppel-Domcke-Cederbaum (KDC) vibronic Hamiltonian calculations. *J. Chem. Phys.* **2017**, *146*, 224309.
(43) Style, D. W. G.; Ward, J. C. Fluorescent spectra from ethyl nitrate. Part I. - Supposed emissions from alkoxy radicals and NO_2. *Trans. Faraday Soc.* **1953**, *49*, 999−1002.
(44) Radford, H. E.; Russell, D. K. Spectroscopic detection of methoxy (CH_3O). *J. Chem. Phys.* **1977**, *66*, 2222−2224.
(45) Russell, D. K.; Radford, H. E. Analysis of the LMR spectra of methoxy, CH_3O. *J. Chem. Phys.* **1980**, *72*, 2750−2759.
(46) Ohbayashi, K.; Akimoto, H.; Tanaka, I. Emission spectra of CH_3O, C_2H_5O, and *i*-C_3H_7O radicals. *J. Phys. Chem.* **1977**, *81*, 798−802.
(47) Inoue, G.; Akimoto, H.; Okuda, M. Spectroscopy of the CH_3O A $^2A_1X^2E$ system by laser-excited fluorescence method. *J. Chem. Phys.* **1980**, *72*, 1769−1775.
(48) Carrick, P. G.; Brossard, S. D.; Engelking, P. C. Experimental observation of the spin-orbit splitting in methoxy. *J. Chem. Phys.* **1985**, *83*, 1995−1996.
(49) Foster, S. C.; Misra, P.; Lin, T. Y. D.; Damo, C. P.; Carter, C. C.; Miller, T. A. The free jet-cooled laser-induced fluorescence spectrum of methoxy. Part I: Vibronic analysis of the $\tilde{A}$ and $\tilde{X}$ states. *J. Phys. Chem.* **1988**, *92*, 5914−5921.
(50) Powers, D. E.; Pushkarsky, M. B.; Miller, T. A. Rovibronic analysis of laser induced fluorescence excitation spectrum of the jet-cooled methoxy radical. *J. Chem. Phys.* **1997**, *106*, 6863−6877.
(51) Liu, X.; Damo, C. P.; Lin, T.-Y.; Foster, S. C.; Misra, P.; Yu, L.; Miller, T. A. The free jet-cooled laser-induced fluorescence spectrum of methoxy. Part II: Rotational analysis of the $\tilde{A}\ ^2A_1 \leftrightarrow \tilde{X}\ ^2E$ electronic transition. *J. Phys. Chem.* **1989**, *93*, 2266−2275.
(52) Geers, A.; Kappert, J.; Temps, F.; Wiebrecht, J. Rotation-vibration state resolved unimolecular dynamics of highly vibrationally excited CH_3O (X ^{2}E). I. Observed stimulated emission pumping spectra. *J. Chem. Phys.* **1994**, *101*, 3618−3633.
(53) Geers, A.; Kappert, A. G. J.; Temps, F.; Wiebrecht, J. Rotation-vibration state resolved unimolecular dynamics of highly vibrationally excited CH_3O (X ^{2}E). II. Intramolecular vibrational dynamics of excited ″C-O stretch″ states. *J. Chem. Phys.* **1994**, *101*, 3634−3648.
(54) Liu, J.; Chen, M.-W.; Melnik, D.; Yi, J. T.; Miller, T. A. The spectroscopic characterization of the methoxy radical (Part I): Rotationally resolved $\tilde{A}^2A_1 - \tilde{X}^2E$ electronic spectra of CH_3O. *J. Chem. Phys.* **2009**, *130*, 074302.
(55) Han, J.; Hu, S.; Chen, H.; Utkin, Y.; Brown, J. M.; Curl, R. F. Jet-cooled infrared spectrum of methoxy in the CH stretching region. *Phys. Chem. Chem. Phys.* **2007**, *9*, 3725−3734.
(56) Momose, T.; Endo, Y.; Hirota, E.; Shida, T. The submillimeter-wave spectrum of the $^{13}CH_3O$ radical. *J. Chem. Phys.* **1988**, *88*, 5338−5343.
(57) Endo, Y.; Saito, S.; Hirota, E. The microwave spectrum of the methoxy radical CH_3O. *J. Chem. Phys.* **1984**, *81*, 122−135.
(58) Marenich, A. V.; Boggs, J. E. A model spin-vibronic Hamiltonian for twofold degenerate electron systems: A variational ab initio study of $\tilde{X}^2E$ CH_3O·. *J. Chem. Phys.* **2005**, *122*, 024308.
(59) Marenich, A. V.; Boggs, J. E. Equation-of-motion coupled-cluster study of Jahn-Teller effect in X^2E CF_3O· and CF_3S·. *Int. J. Quantum Chem.* **2006**, *106*, 2609−2616.
(60) Marenich, A. V.; Boggs, J. E. The molecular structure, spin-vibronic energy levels, and thermochemistry of CH_3O. *J. Mol. Struct.* **2006**, *780*, 163−170.
(61) Nagesh, J.; Sibert, E. L. Vibrational dynamics around the conical intersection: A study of methoxy vibrations on the $\tilde{X}^2E$ surface. *Phys. Chem. Chem. Phys.* **2010**, *12*, 8250−8259.
(62) Dillon, J.; Yarkony, D. R. Nonadiabatic effects in substitutional isomers of Jahn-Teller molecules: The strange case of hydroxymethoxy. *J. Chem. Phys.* **2012**, *137*, 154315.
(63) Johnson, B. A.; Sibert, E. L. Assigning the low lying vibronic states of CH_3O and CD_3O. *J. Chem. Phys.* **2017**, *146*, 174112.
(64) Shao, Z.; Mo, Y. Jahn-Teller effect in $CH_2DO/CHD_2O(\tilde{X}^2E)$: Vibronic coupling of all vibrational modes. *J. Chem. Phys.* **2013**, *138*, 244309.
(65) Deev, A.; Sommar, J.; Okumura, M. Cavity ringdown spectrum of the forbidden $\tilde{A}^2E'' \leftarrow \tilde{X}^2A_2$ transition of NO_3: Evidence for static Jahn-Teller distortion in the $\tilde{A}$ state. *J. Chem. Phys.* **2005**, *122*, 224305.
(66) Okumura, M.; Stanton, J. F.; Deev, A.; Sommar, J. New insights into the Jahn-Teller effect in NO_3 via the dark $\tilde{A}^2E''$ state. *Phys. Scr.* **2006**, *73*, C64−C70.
(67) Stanton, J. F.; Okumura, M. On the vibronic level structure in the NO_3 radical part III. Observation of intensity borrowing via ground state mixing. *Phys. Chem. Chem. Phys.* **2009**, *11*, 4742−4744.
(68) Takematsu, K.; Eddingsaas, N. C.; Robichaud, D. J.; Okumura, M. Spectroscopic studies of the Jahn-Teller effect in the $\tilde{A}^2E''$ state of the nitrate radical NO_3. *Chem. Phys. Lett.* **2013**, *555*, 57−63.
(69) Codd, T.; Chen, M.-W.; Roudjane, M.; Stanton, J. F.; Miller, T. A. Jet cooled cavity ringdown spectroscopy of the $\tilde{A}^2E'' \leftarrow \tilde{X}^2A'_2$ transition of the NO_3 radical. *J. Chem. Phys.* **2015**, *142*, 184305.
(70) Weaver, A.; Arnold, D. W.; Bradforth, S. E.; Neumark, D. M. Examination of the $^2A'_2$ and $^2E''$ states of NO_3 by ultraviolet photoelectron spectroscopy of NO_3^-. *J. Chem. Phys.* **1991**, *94*, 1740−1751.
(71) Eisfeld, W.; Morokuma, K. *Ab Initio* investigation of the vertical and adiabatic excitation spectrum of NO_3. *J. Chem. Phys.* **2001**, *114*, 9430−9440.
(72) Eisfeld, W.; Vieuxmaire, O.; Viel, A. Full-dimensional diabatic potential energy surfaces including dissociation: The ^{2}E state of NO_3. *J. Chem. Phys.* **2014**, *140*, 224109.
(73) Faraji, S.; Köppel, H.; Eisfeld, W.; Mahapatra, S. Towards a higher-order description of Jahn-Teller coupling effects in molecular spectroscopy: The $\tilde{A}^2E''$ state of NO_3. *Chem. Phys.* **2008**, *347*, 110−119.
(74) Mahapatra, S.; Eisfeld, W.; Koeppel, H. Effects of multimode Jahn-Teller coupling on the photodetachment spectrum of nitrate anion (NO_3^-). *Chem. Phys. Lett.* **2007**, *441*, 7−15.
(75) Stanton, J. F. On the vibronic level in the NO_3 radical: II. Adiabatic calculation of the infrared spectrum. *Mol. Phys.* **2009**, *107*, 1059−1075.

DOI: 10.1021/acs.jpca.9b03360
J. Phys. Chem. A 2019, 123, 4990−5004